A new multi-target tracking algorithm for a large number of orbiting objects

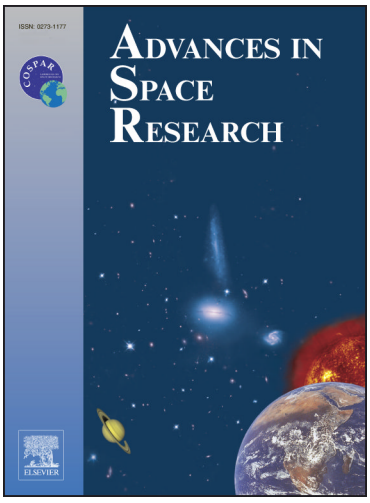

A new multi-target tracking algorithm for a large number of orbiting objects

E. Delande, J. Houssineau, J. Franco, C. Frueh, D. Clark, M. Jah

PII: S0273-1177(19)30272-8
DOI: https://doi.org/10.1016/j.asr.2019.04.012
Reference: JASR 14217

To appear in: *Advances in Space Research*

Received Date: 2 February 2019
Revised Date: 8 April 2019
Accepted Date: 10 April 2019

Please cite this article as: Delande, E., Houssineau, J., Franco, J., Frueh, C., Clark, D., Jah, M., A new multi-target tracking algorithm for a large number of orbiting objects, *Advances in Space Research* (2019), doi: https://doi.org/10.1016/j.asr.2019.04.012

A new multi-target tracking algorithm for a large number of orbiting objects

E. Delande[a,*], J. Houssineau[b], J. Franco[c], C. Frueh[d], D. Clark[e], M. Jah[f]

[a]*Institute for Computational Engineering and Sciences, The University of Texas at Austin, USA.*
[b]*Department of Statistics and Applied Probability, National University of Singapore, Singapore.*
[c]*School of Engineering & Physical Sciences, Heriot-Watt University, United Kingdom.*
[d]*School of Aeronautics & Astronautics, Purdue University, USA.*
[e]*Département CITI, Telecom SudParis, France.*
[f]*Department of Aerospace Engineering and Engineering Mechanics, The University of Texas at Austin, USA.*

Abstract

This paper presents the filter for Hypothesised and Independent Stochastic Populations (HISP), a multi-object joint detection/tracking algorithm derived from a recent estimation framework for stochastic populations, in the context of Space Situational Awareness. Designed for multi-object estimation problems where the data association between tracks and collected observations is moderately ambiguous, the HISP filter has a linear complexity with the number of objects and the number of observations. Because of its scalable complexity, the HISP filter is a promising solution for the construction of a large-scale catalogue of Resident Space Objects. We illustrate the HISP filter on a challenging surveillance scenario built from real data for 115 satellites of PlanetLabs' Dove constellation, and simulated observations collected from two sensors with limited coverage and measurement noise, in the presence of false positives and missed detection.

Keywords: Multi-object Bayesian estimation, multi-target detection and tracking, stochastic populations, space situational awareness

1. Introduction

One of the main objectives of Space Situational Awareness (SSA) activities is the construction of an up-to-date catalogue identifying and describing all the objects orbiting around Earth - the so called Resident Space Objects (RSOs) – supported by general knowledge about orbital mechanics and data collected from various physics-based sensors (e.g. telescopes, radars), human-based statements (e.g. launch event described on a website), or data sources mixing physics- and human-based elements such as the Two-Line Elements (TLEs) maintained by the U.S. Strategic Command (USStratCom). Many features can be incorporated in what constitutes an adequate description – or *state* – of an individual RSO, depending on the interests of the end-users exploiting a specific catalogue. The state (almost) always contains a kinematic description of the RSO (position, velocity coordinates in a suitable reference frame), sometimes augmented with other uncertain parameters affecting the orbital mechanics, such as the RSO's ballistic coefficient and/or Area-To-Mass Ratio (AMR).

Maintaining an up-to-date catalogue of RSOs entails many challenges, increasingly so with the number of RSOs in the near-Earth space mostly due to human activity. The main problems can be stated as follows:

- The number of RSOs is unknown and time-varying;
- The nature and importance of the physical perturbations affecting orbital trajectories are not fully understood;
- The collected data has limited observability, precision, and accuracy, due to physical limitations of the data sources;
- The association between RSOs and the collected data is usually ambiguous.

*Corresponding author
Email addresses: edelande@ices.utexas.edu (E. Delande), stahje@nus.edu.sg (J. Houssineau), jf139@hw.ac.uk (J. Franco), cfrueh@purdue.edu (C. Frueh), daniel.clark@telecom-sudparis.eu (D. Clark), moriba@utexas.edu (M. Jah)

Estimating the size *and* individual states of a population of objects, under the conditions listed above, is known as a multi-object estimation problem. It has been studied extensively for several decades in the tracking community, though applications to the context of SSA remain relatively scarce. It is usually approached within the context of Bayesian filtering, in which a probabilistic representation of the population of objects is propagated through time and sequentially updated whenever a new piece of data is available.

The design of modern approaches to the multi-object Bayesian estimation problem started in the late 1970s with the first *track-based* algorithms Reid (1979), whose development has continued ever since Bar-Shalom and Li (1995), Blackman (2004). Track-based solutions follow an intuitive approach, where the existence of an object is inferred from a sequence of coherent observations collected across time, forming a *track*. A track is identified by its sequence of observations, and describes the individual state of the corresponding object through a suitable probabilistic representation, usually a probability density function (p.d.f.) on some object state space. The most popular track-based algorithm is perhaps the Multiple Hypothesis Tracking (MHT) Reid (1979), Blackman (2004), which hypothesizes the existence of objects through the exploration of every possible track-to-observation association. A well-known issue of the MHT, or similar track-based approaches, is their prohibitive computational cost in large scale scenarios due to the combinatorial nature of the track-to-observation association process. Ad-hoc procedures exist to discard unlikely candidate tracks, similar to the "m-out-of-n rule" when tracks are generated from a surveillance radar Skolnik (1979), but the MHT lacks a robust, principled approximation alleviating the combinatorics in the data track-to-observation process for large scale scenarios.

The need for a more systematic, principled approach in the construction of *approximated* multi-object Bayesian estimation algorithms adapted to large scale scenarios led to the emergence of point-process-based Washburn (1987) or set-based Goodman et al. (1997); Mahler (2007) approaches. Unlike track-based approaches, set-based solutions do not hypothesize the existence of individual objects through as many individual tracks; instead, they propagate the distribution of a Random Finite Set (RFS), a random object whose size and elements are both random and describe the number of objects and their states, respectively Mahler (2007). Early set-based solutions, such as the Probability Hypothesis Density (PHD) filter Mahler (2007), represent the population of objects with a single RFS. They do not maintain individual statistics on objects or track custody along the filtering process, but the data association step does not involve combinatorics since pairings between individual objects and individual observations become unnecessary. Applications of set-based solutions to the context of SSA can be found in Hussein et al. (2012); DeMars et al. (2015); Faber et al. (2016). The tracking community then focused on addressing challenging scenarios where maintaining individual information on objects is a requisite, even at the cost of more computationally demanding solutions. Recent developments keep track of individual objects through *labeled* RFSs Vo and Vo (2013), a random object derived from the RFS in which the elements are systematically labeled. Recent applications to the context of SSA can be found in Jones and Vo (2015); Jones et al. (2016).

We propose in this paper the filter for Hypothesised and Independent Stochastic Populations (HISP) Houssineau and Clark (2018), a recent solution that presents several advantages in the context of large scale scenarios. First, it stems from the estimation framework for stochastic populations Houssineau (2015); Houssineau and Clark (2019), an alternative to the approaches above that introduces the concept of object *distinguishability* in order to avoid combinatorics as much as possible. Similarly to a RFS representation, when a group of objects remain unidentifiable from one another because no specific information is available on any one of them, they form a population of *indistinguishable* individuals that induces no combinatorics in data association events. Similarly to usual track-based approaches, an object that is identified through specific information becomes *distinguishable* and is described by its own track. Second, the HISP filter was specifically derived as an approximate, scalable solution whose filtering mechanisms have linear complexity in the number of objects and observations. Non-linear operations are limited to the track extraction process, a mechanism that is independent from filtering and can be operated offline in most practical cases.

The HISP filter has already been successfully exploited in the context of SSA and presented at the 2017 AAS/AIAA Spaceflight Mechanics Meeting in Delande et al. (2017). This follow-up paper provides a more comprehensive description of the HISP filter,

integrates dynamical behaviors to the object identification process, and extends the 30-object simulated scenario to a more realistic and challenging 115-object scenario, generated from GPS points collected from PlanetLabs' constellation of Dove satellites.

The structure of the paper is as follows. The key features of the estimation framework for stochastic populations are given in Section 2, and the HISP filter is presented in Section 3. A practical implementation of a SSA scenario is detailed in Section 4, and Section 5 concludes.

2. The estimation framework for stochastic populations

This section describes the estimation framework for stochastic populations, and exposes key modeling assumptions leading to the HISP filter. A more comprehensive description of the framework and the HISP filter, including mathematical proofs, can be found in Houssineau (2015) and Houssineau and Clark (2018), respectively.

2.1. Surveillance scene and object state space

A multi-object estimation problem concerns itself with some objects of interest – or *targets* – evolving in some bounded region of the physical space called the *surveillance scene*. In the context of a comprehensive catalogue for SSA, the objects of interest are the RSOs and the surveillance scene is the region of near-Earth space relevant to SSA activities, i.e., the region whose lower altitudes are delimited by the upper regions of the atmosphere, and higher altitudes include the geosynchronous orbits. We assume that every object in the scene possesses some individual characteristics of interest (position, velocity coordinates in a suitable frame, etc.) and described by a *state* in some d-dimensional subset $\mathbf{X} \subseteq \mathbb{R}^d$ called the object state space.

In many realistic multi-object estimation problems the presence of an object in the surveillance scene at any time is uncertain, as it may enter or leave the scene through its physical boundaries (consider, for example, a newly launched satellite or the atmosphere re-entry of a decommissioned spacecraft). From the perspective of filtering it is convenient to consider the existence of objects as perpetual and disconnected with their physical lifetime, and to assume that an object has the "empty" state ψ when it is *not* in the surveillance scene. The *(full) object state space* is then given by $\bar{\mathbf{X}} = \{\psi\} \cup \mathbf{X}$.

2.2. Tracks and stochastic population

In a typical multi-object estimation problem, the number of objects of interest is unknown. Some pieces of information are specific to an individual object – for example, the reported launch of one satellite, or an observation extracted from a radar scan – some refer to a group of objects whose size might be uncertain – for example, a reported collision creating an unknown number of pieces of debris. In the filtering process, the existence of one or several objects is hypothesized through a coherent stream of collected evidence or *track*. By construction, the same information is available on each of the potential objects represented by a given track. An explicit identification of these objects – through a label, for example – offers little operational gain, but introduces unnecessary and artificial combinatorics in data association events.[1]

In the considered framework, each track *collectively* represents the information maintained on the state of *each* of the objects in the sub-population it represents, and these objects are *indistinguishable* from one another for the purpose of estimation[2]. One track could represent, say, the information on a cloud of debris resulting from a collision, before individual observations identifying specific pieces of debris become available; another track could represent *one* satellite on which specific information is available. Throughout the filtering process, tracks are identified by indices in some index set $\mathbb{I}$, a countable set whose nature will be discussed in Section 2.3. A possible composition of the population is given by a *configuration* $\mathbf{n} \in \mathbb{N}^{\mathbb{I}}$, i.e., a family of integers indexed by $\mathbb{I}$ indicating that the i-th track represents $\mathbf{n}^i$ objects, for any $i \in \mathbb{I}$. The integer $\mathbf{n}^i$ is referred to as the *multiplicity* of the i-th track in the configuration $\mathbf{n}$.

In the general case, the composition of the population of interest is uncertain and the existence of individual tracks are dependent from another, most notably because associations to observations collected from physical sensors are typically exclusive. The composition of the population is hypothesised through a probability mass function (p.m.f.) $\mathbf{w}$ on $\mathbb{N}^{\mathbb{I}}$, i.e., a non-negative function on $\mathbb{N}^{\mathbb{I}}$ such that

$$\sum_{\mathbf{n} \in \mathbb{N}^{\mathbb{I}}} \mathbf{w}(\mathbf{n}) = 1, \tag{1}$$

[1] This is further discussed in Example 1 later in this section.

[2] If more information is later collected on this sub-population, however, its individual members may become *distinguishable* from one another.

where $\mathbf{w}(\mathbf{n})$ is the probability that the composition of the population is given by the configuration $\mathbf{n} \in \mathbb{N}^{\mathbb{I}}$. The hypothesised size of the i-th sub-population can be retrieved through the marginalization

$$\mathbf{w}^i(n) = \sum_{\substack{\mathbf{n}\in\mathbb{N}^{\mathbb{I}} \\ \mathbf{n}^i=n}} \mathbf{w}(\mathbf{n}), \tag{2}$$

for any $n \in \mathbb{N}$. If the multiplicity of some track $i \in \mathbb{I}$ is less than one with probability one, i.e., if $\mathbf{w}^i(0) + \mathbf{w}^i(1) = 1$, then this track represents *at most one* object in the population, and this object becomes *distinguishable* [3].

The nature of the stochastic population evolves throughout the filtering process and the acquisition of information on the population of interest. This process is reflected in three main mechanisms:

1. the identification of tracks, through the set of index $\mathbb{I}$;
2. the estimation of the tracks' states, through their probability distributions;
3. the estimation of the population's composition, through the p.m.f. $\mathbf{w}$.

Sections 2.3 and 2.4 focus on the identification of tracks and the estimation of the tracks' states, respectively. The estimation of the population's composition, by far the most computationally challenging mechanism of a multi-object filter, is covered in Section 3.

2.3. Filtering decisions and track identification

The considered framework is set within the Bayesian paradigm, and the stochastic population is transformed throughout a sequence of *time-update* and *data-update* steps. Tracks are formed throughout *filtering decisions*, corresponding to hypothesized behavior patterns in the time-update steps, and to hypothesized associations with collected observations in the data-update steps. Without loss of generality, the time is indexed by the natural integers $\mathbb{N}$ where an index $t \in \mathbb{N}$ corresponds to an epoch where filtering decisions are made.

[3] Roughly speaking, if the p.m.f. $\mathbf{w}$ is such that all the objects are distinguishable from one another, then every object is identified with a unique label as in track-based or labeled RFS-based solutions. On the other hand, if the mass of the p.m.f. $\mathbf{w}$ is concentrated on a single element of $\mathbb{I}$, then all the objects are indistinguishable from one another as in the PHD filter, or in any other set-based solutions propagating a single identically and independently distributed (i.i.d.) RFS.

2.3.1. Time-update decisions

Filtering decisions made during the time-update step relate to the operator's knowledge about behavior patterns affecting the dynamics of an object. At any time $t \in \mathbb{N}$, the patterns describing possible dynamical behaviors between time $t-1$ and t are indexed by a *set of motion models* M_t. Some models may correspond to broad, generic patterns drawn from general knowledge on the population of interest – for example, a stable Low-Earth Orbit (LEO) orbital trajectory – while other models may be opportunistic and based on some specific event in time – for example, a reported launch with a specific payload. For the purpose of filtering, it is convenient to consider an "away" motion model m^ψ applying to all the objects outside of the surveillance scene between $t-1$ and t, and we denote by $\bar{M}_t = \{m^\psi\} \cup M_t$ the *(full) set of motion models*. An important feature participating in the identification of objects is their history of behavior patterns. We consider the space $\bar{\mathbb{B}}_t$, defined as the Cartesian product

$$\bar{\mathbb{B}}_t = \bar{M}_0 \times \cdots \times \bar{M}_t, \tag{3}$$

so that $\mathbf{b}_t \in \bar{\mathbb{B}}_t$ takes the form $\mathbf{b}_t = (m_0, \ldots, m_t)$ with $m_{t'} \in \bar{M}_{t'}$, for any $0 \leq t' \leq t$. A sequence $\mathbf{b}_t$ corresponds to a sequence of time-update decisions and is referred to as a *behavior history*. The "away" behavior history $\left(m^\psi, \ldots, m^\psi\right) \in \bar{\mathbb{B}}_t$ is denoted by $\boldsymbol{m}_t^\psi$.

2.3.2. Data-update decisions

Filtering decisions made during the data-update step relate to the processing of the collected observations, each providing information on the current state of an object. We denote by $\mathbf{Z}_t \subseteq \mathbb{R}^{d'_t}$ the d'_t-dimensional observation space at time $t \in \mathbb{N}$, describing the measurable quantities collected in one observation (e.g. range, azimuth, elevation, and range rate for a radar with Doppler effect), and by Z_t the set of observations in $\mathbf{Z}_t$ collected from the data source. From a filtering perspective, it is convenient to introduce an "empty observation" ϕ to denote missed detection; we then denote by $\bar{\mathbf{Z}}_t = \{\phi\} \cup \mathbf{Z}_t$ and $\bar{Z}_t = \{\phi\} \cup Z_t$ the *(full) observation state space* and the *(full) set of observations*, respectively. Similarly to behavior histories, we consider the space $\bar{\mathbb{O}}_t$, defined as the Cartesian product

$$\bar{\mathbb{O}}_t = \bar{Z}_0 \times \cdots \times \bar{Z}_t, \tag{4}$$

so that $\mathbf{o}_t \in \bar{\mathbb{O}}_t$ takes the form $\mathbf{o}_t = (z_0, \ldots, z_t)$ with $z_{t'} \in \bar{Z}_{t'}$, for any $0 \leq t' \leq t$. A sequence $\mathbf{o}_t$

corresponds to a sequence of data-update decisions and is also referred to as an *observation history* or *observation path*. The "empty" observation history $(\phi, \dots, \phi) \in \bar{\mathbb{O}}_t$ is denoted by $\boldsymbol{\phi}_t$.

2.3.3. Track identification

The existence of objects in the population is inferred solely through the information described by the filtering decisions, and a possible track is identified by the conjunction of one behavior history and one observation history. At any time $t \in \mathbb{N}$, the set of all possible track indices is then given by $\bar{\mathbb{B}}_t \times \bar{\mathbb{O}}_{t-1}$ following the time-update step, and by $\bar{\mathbb{B}}_t \times \bar{\mathbb{O}}_t$ following the data-update step.

In the most general case, there is no one-to-one correspondence between individual observations and individual objects[4]. However, the HISP filter relies on the modeling assumptions that, at any time $t \in \mathbb{N}$:

M.1 An object produces at most one observation (if not, a *missed detection* occurs),

M.2 An observation originates from at most one object (if not, it is a *false positive*).

An important consequence of Assumptions **M**.1, **M**.2 is that any track $i = (\mathbf{b}_t, \mathbf{o}_t)$, where $\mathbf{o}_t$ is a non-empty observation path in $\bar{\mathbb{O}}_t \setminus \{\boldsymbol{\phi}_t\}$, describes at most one object in the population of interest: objects become distinguishable through observations. These assumptions are reasonable in many tracking problems, especially when the typical size of the objects is no larger than the typical resolution of the sensors observing the scene.

On the other hand, usual motion models are broad behavior patterns that do not relate to a specific individual: evolving along a stable LEO trajectory, for example, is not an exclusive behavior pattern that relates to a single RSO. A similar assumption as **M**.2 does not hold for time-update decisions, then, and objects do not become distinguishable through behavior patterns in the general case. Notable exceptions occur, such as the scheduled launch of a single RSO (see example below).

Example 1. *At time $t = 0$, the operator knows about two launching events. One involves a single satellite, represented by the model $m_0^1 \in M_0$, the other an unknown number of satellites, represented by the model $m_0^2 \in M_0$. The operator maintains the following tracks:*

- $\big(m_0^1, \phi\big)$, *for* the *RSO launched with the first event;*
- $\big(m_0^2, \phi\big)$, *for the sub-population of RSOs launched with the second event.*

At time $t = 1$, the operator knows that the newly launched objects stay on their initial orbit, represented by the model $m_1^1 \in M_1$. Besides, a single observation z_1 of unknown origin is collected by a radar. The operator then maintains the following tracks:

- $\big((m_0^1, m_1^1), (\phi, z_1)\big)$, *for* the *RSO launched from the first event and detected with z_1;*
- $\big((m_0^1, m_1^1), (\phi, \phi)\big)$, *for* the *RSO launched from the first event and undetected at $t = 1$;*
- $\big((m_0^2, m_1^1), (\phi, z_1)\big)$, *for* the *RSO launched from the second event and detected with z_1;*
- $\big((m_0^2, m_1^1), (\phi, \phi)\big)$, *for the sub-population of RSOs launched from the second event and undetected at $t = 1$.*

*The first launch is, by definition, an example of behavior specific to one RSO. So is the radar detection, by virtue of Assumptions **M**.1, **M**.2. The filtering decisions associated to these events each relate to a unique RSO, but the other events do not. If the radar detection z_1 distinguishes one RSO from the sub-population $\big((m_0^2, m_1^1), \phi\big)$, hypothesized from the second launch and propagated to $t = 1$, it does* not *matter which one. For estimation purposes, these RSOs are indistinguishable and there is only* one way *to associate the sub-population $\big((m_0^2, m_1^1), \phi\big)$ with the observation z_1.*

We see in the example above that individual objects are identified in the stochastic population only when the information acquired on them allows us to do so. There is a only one way to associate observations to a sub-population of objects *indistinguishable* from one another, and thus combinatorics are only involved in the association between observations and *distinguishable* objects. There are fundamental implications on the complexity of the filters derived from the considered framework Houssineau (2015), but they are left out of the scope of this paper.

2.4. Single object Bayesian filtering

We now focus on the estimation of the tracks' states, and describe the single-object Bayesian filtering equations at time $t \in \mathbb{N}$, for a possible track

[4]For example, extended object tracking problems focus on tracking applications where one object may produce several observations per sensor scan.

$(\mathbf{b}_{t-1}, \mathbf{o}_{t-1}) \in \bar{\mathbb{B}}_{t-1} \times \bar{\mathbb{O}}_{t-1}$ associated to some motion model $m \in \bar{M}_t$ and some observation $z \in \bar{Z}_t$. The mechanism is similar to usual track-based approaches and relies on the standard multi-object filtering model, i.e.

M.3 Objects evolve independently from one another;

M.4 Observations originating from objects are generated independently from one another.

Assumptions **M**.3, **M**.4 imply that the information maintained on the state of track $(\mathbf{b}_{t-1}, \mathbf{o}_{t-1})$ depends only on its behavior history $\mathbf{b}_{t-1}$ and its observation history $\mathbf{o}_{t-1}$.

2.4.1. Time-update step

We assume that the information on the state of track $(\mathbf{b}_{t-1}, \mathbf{o}_{t-1})$ is given by some probability distribution $p_{t-1}^{(\mathbf{b}_{t-1}, \mathbf{o}_{t-1})}$ on the full object state space $\bar{\mathbf{X}}$. The probability distribution admits a density on the continuous part of the state space, and the resulting p.d.f. is denoted the same way[5]. The state of the time-updated track $((\mathbf{b}_{t-1}, m), \mathbf{o}_{t-1})$ is then described by

$$p_{t|t-1}^{((\mathbf{b}_{t-1}, m), \mathbf{o}_{t-1})}(x) \propto \int q_m(x|x') p_{t-1}^{(\mathbf{b}_{t-1}, \mathbf{o}_{t-1})}(x') \mathrm{d}x', \tag{5}$$

for any $x \in \bar{\mathbf{X}}$, where $q_m(x|x')$ is the transition kernel describing the motion model m such that $\int q_m(x|x')\mathrm{d}x \leq 1$ for any object state $x' \in \bar{\mathbf{X}}$.

2.4.2. Data-update step

Likewise, the state of the data-updated track $(\mathbf{b}_t, (\mathbf{o}_{t-1}, z))$ is described by

$$p_t^{(\mathbf{b}_t, (\mathbf{o}_{t-1}, z))}(x) = \frac{\ell_t(z|x) p_{t-1}^{(\mathbf{b}_t, \mathbf{o}_{t-1})}(x)}{\int \ell_t(z|x') p_{t-1}^{(\mathbf{b}_t, \mathbf{o}_{t-1})}(x') \mathrm{d}x'}, \tag{6}$$

for any $x \in \bar{\mathbf{X}}$, where $\ell_t(\cdot|x)$ is the likelihood describing the data source that produced observation z, given by

$$\ell_t(z|x) = \begin{cases} 1, & \text{if } z = \phi, x = \psi \\ 0, & \text{if } z \in \mathbf{Z}_t, x = \psi \\ 1 - p_{\mathrm{d},t}(x), & \text{if } z = \phi, x \in \mathbf{X} \\ p_{\mathrm{d},t}(x) g_t(z|x), & \text{if } z \in \mathbf{Z}_t, x \in \mathbf{X}, \end{cases} \tag{7}$$

where $0 \leq p_{\mathrm{d},t}(x) \leq 1$ is the probability of detection of an object with state x, and the function $g_t(\cdot|x)$ on $\mathbf{Z}_t$ is a potential describing the precision/accuracy of the data source. In the usual Bayesian filtering context, the sensor's observation process is represented with a random variable and the potential $g_t(\cdot|x)$ takes the form of a p.d.f. on $\mathbf{Z}_t$. In the implementation of the HISP filter, detailed in Section 4.2, we will follow a different approach based on an alternative representation of uncertain phenomena Houssineau (2018); Houssineau and Bishop (2018) that we have already exploited in the context of SSA Delande et al. (2018c,b).

[5]The same assumption and naming convention will apply to all probability distributions in the paper.

3. The HISP filter: principle and core mechanisms

Assessing the composition of the population of objects is a core mechanism of a multi-object filter, and often results from a trade-off between the quality of the propagated information and the incurred computational cost. Our initial works in the context of SSA involved the filter for Distinguishable and Independent Stochastic Populations (DISP) Delande et al. (2016), a robust solution adapted to challenging scenarios and designed to address a similar class of problems as the MHT Blackman (2004) or the labeled multi-Bernoulli filter Vo and Vo (2013). It maintains a large number of individual tracks and incurs a high computational cost due to the combinatorics in the exploration of track-to-observation associations, limiting its applicability to large-scale SSA scenarios Delande et al. (2018a). The HISP filter is a principled approximation of the DISP filter, simplifying its data-update step to maintain a linear complexity in the number of tracks and observations Houssineau and Clark (2018).

We discuss the key assumptions of the HISP filter in Section 3.1, and present its filtering equations in Sections 3.2 and 3.3 for the time-update and data-update step, respectively. Section 3.4 proposes a mechanism to extract a population estimate from the filter's output, and Section 3.5 presents several approximations improving its computational efficiency.

3.1. Population management: simplifying assumptions

As seen in Section 2.3, the number of possible track indices in $\bar{\mathbb{B}}_t \times \bar{\mathbb{O}}_t$ increases linearly with the number of motion models, and with the number of observations, available at each decision time $t \in \mathbb{N}$. However, since the existence of individual tracks are not independent from one another in the general

case[6], the p.m.f. $\mathbf{w}_t$ describing the composition of the population (1) must account for the joint probability of existence of tracks and has a far more complex structure.

3.1.1. Track independence

The HISP filter relies on the simplifying assumption that

S.1 The tracks are independent from one another.

Assumption **S**.1 implies that the p.m.f. $\mathbf{w}_t$ admits a simpler structure than in the general form (1), where the individual multiplicities (2) can be marginalized and propagated for each track. As it will be seen in Sections 3.2 and 3.3, it is a key element in the time-update and data-update mechanisms of the HISP filter.

3.1.2. Indistinguishable objects

Since no specific information is available on any indistinguishable object, either through observations or scheduled behavior events, information on sub-populations of indistinguishable objects is by nature scarce. Propagating several of them has little benefit in many practical scenarios, and the HISP filter assumes that

S.2 All the indistinguishable objects are represented by a single sub-population.

There is therefore a single track, represented by the index $\mathrm{u}_t \in \mathbb{I}_t$, that describes all the objects in the scene that are unidentified so far. The expression of u_t as an element of $\bar{\mathbb{B}}_t \times \bar{\mathbb{O}}_t$ will be discussed later on.

3.1.3. Stochastic population

As a consequence of the independence of tracks, the HISP filter maintains information on each track in $\mathbb{I}_t$ separately from one another. At any time $t \in \mathbb{N}$, the stochastic population maintained by the HISP filter is of the simpler form

$$\{w_t^i, n_t^i, p_t^i\}_{i \in \mathbb{I}_t}, \tag{8}$$

where:

- $\mathbb{I}_t \subseteq \bar{\mathbb{B}}_t \times \bar{\mathbb{O}}_t$ is the set of index tracks (including the indistinguishable track u_t)
- $0 \leq w_t^i \leq 1$ is the *probability of existence* or *weight* of the i-th track, describing its credibility;
- n_t^i is the multiplicity of the i-th track, describing the number of objects it represents;
- p_t^i is the p.d.f. of the i-th track, describing its state in $\bar{\mathbf{X}}$.

In particular, $n_t^{\mathrm{u}_t}$ provides some information on the number of unidentified objects in the scene while $w_t^{\mathrm{u}_t}$ assesses the existence of each unidentified individual. The information on unidentified objects is limited, and the indistinguishable objects will be only exploited as a "pool" from which new tracks are produced out of collected observations. Any other track $i = (\mathbf{b}_t, \mathbf{o}_t) \in \mathbb{I}_t \setminus \{\mathrm{u}_t\}$ represents a distinguishable object. It has a multiplicity of $n_t^i = 1$ by construction, and its weight w_t^i reflects the confidence of the filter in the existence of an object, in the population of interest, with behavior history $\mathbf{b}_t$ and observation history $\mathbf{o}_t$.

3.2. Time-update step

We now detail the time-update step of the HISP filter, at an arbitrary time step $t \in \mathbb{N}$. The behavior patterns M_t describing the dynamics of the objects are as follows:

- Some evolution models $M_t^{\mathrm{e}} \subset M_t$ describe objects evolving in the scene;
- A unique "death" model $m_t^{\mathrm{d}} \in M_t$ describes objects leaving the scene;
- Some "identified birth" models $M_t^{\mathrm{b}} \subset M_t$, describe specific objects entering the scene;
- A unique "unidentified birth" model $m_t^{\mathrm{ub}} \in M_t$ describes unidentified objects entering the scene.

3.2.1. Evolution and death models

An evolution model $m_t^{\mathrm{e}} \in M_t^{\mathrm{e}}$ represents a general behavior pattern followed since last epoch $t-1$ – for example, a stable orbital trajectory. This model does not consider objects leaving the scene, that is, an object in the scene cannot move to the away state ψ under m_t^{e}. The transition kernel $q_{m_t^{\mathrm{e}}}$ in (5) is thus such that $q_{m_t^{\mathrm{e}}}(\psi|x) = 0$ for any $x \in \mathbf{X}$, and $q_{m_t^{\mathrm{e}}}(\psi|\psi) = 1$.

Similarly, the death model m_t^{d} represents the dynamics of an object that leaves scene between epochs $t-1$ and t. It does not consider objects that were *already* outside of the scene at time $t-1$, and the transition $q_{m_t^{\mathrm{d}}}(\cdot|\psi)$ is such that $\int q_{m_t^{\mathrm{d}}}(x|\psi)\mathrm{d}x = 0$.

[6] For example, since each observation cannot originate from more than one individual under Assumption **M**.2, two distinct tracks sharing an observation cannot *both* represent an object in the population of interest, and therefore cannot exist simultaneously.

On the other hand, objects leaving the scene move to the away state ψ; thus, for any $x \in \mathbf{X}$, the transition kernel $q_{m_t^{\mathrm{d}}}(\cdot|x)$ concentrates its mass towards the away state ψ, i.e., $\int_{\mathbf{X}} q_{m_t^{\mathrm{d}}}(x'|x)\mathrm{d}x' = 0$.

The scalar $p_{m_t^{\mathrm{e}}}(x) = \int_{\mathbf{X}} q_{m_t^{\mathrm{e}}}(x'|x)\mathrm{d}x'$ describes the probability that an object with state $x \in \bar{\mathbf{X}}$ at time $t-1$ has evolved according to m_t^{e}, while the scalar $p_{m_t^{\mathrm{d}}}(x) = q_{m_t^{\mathrm{d}}}(\psi|x)$ describes the probability that it has left the scene. It is assumed that

$$p_{m_t^{\mathrm{d}}}(x) + \sum_{m \in M_t^{\mathrm{e}}} p_m(x) = 1, \tag{9}$$

for any $x \in \mathbf{X}$, i.e., an object in the scene at time $t-1$ has either left the scene by time t, or moved in the scene according to one of the known behavior patterns.

A distinguishable track $(\mathbf{b}_{t-1}, \mathbf{o}_{t-1}) \in \mathbb{I}_{t-1} \setminus \{\mathrm{u}_{t-1}\}$ associated to a behavior pattern $m \in M_t^{\mathrm{e}} \cup \{m_t^{\mathrm{d}}\}$ yields the predicted track $((\mathbf{b}_{t-1}, m), \mathbf{o}_{t-1}) \in \bar{\mathbb{B}}_t \times \bar{\mathbb{O}}_{t-1}$, whose probability distribution is given by the time-update equation (5). Its probability of existence is affected by the credibility of the behavior pattern m and is given by

$$w_{t|t-1}^{((\mathbf{b}_{t-1},m),\mathbf{o}_{t-1})} = \left[\int p_m(x) p_{t-1}^{(\mathbf{b}_{t-1},\mathbf{o}_{t-1})}(x)\mathrm{d}x\right] w_{t-1}^{(\mathbf{b}_{t-1},\mathbf{o}_{t-1})}, \tag{10}$$

while its multiplicity remains unchanged (i.e., $n_{t|t-1}^{((\mathbf{b}_{t-1},m),\mathbf{o}_{t-1})} = n_{t-1}^{(\mathbf{b}_{t-1},\mathbf{o}_{t-1})} = 1$). Predicted tracks that are still in the scene (i.e., if $m \in M_t^{\mathrm{e}}$) are added to the time-updated set of tracks $\mathbb{I}_{t|t-1}$, while those who have left (i.e., if $m = m_t^{\mathrm{d}}$) are not, since they are no longer of interest for filtering purposes. We will see in Section 3.4 that they play a role in the track extraction process, and they must be stored as well. We denote by $\mathbb{I}_t^{\mathrm{d}}$ the set of tracks that have left the scene no later than time t.

3.2.2. Identified birth models

An "identified birth" model $m_t^{\mathrm{b}} \in M_t^{\mathrm{b}}$ represents specific information related to a single object entering the scene between epochs $t-1$ and t. In the context of SSA, a typical example is the report of the successful launch of a satellite. We assume that the state of the newborn object is described by some p.d.f. $q_{m_t^{\mathrm{b}}}$ on $\bar{\mathbf{X}}$. Since the newborn object has entered the scene no earlier than time $t-1$, we assume that it is still in the scene at time t and thus $q_{m_t^{\mathrm{b}}}(\psi) = 0$. A new track indexed by $i = \left((\boldsymbol{m}_{t-1}^{\psi}, m_t^{\mathrm{b}}), \boldsymbol{\phi}_{t-1}\right) \in \bar{\mathbb{B}}_t \times \bar{\mathbb{O}}_{t-1}$ is then added to the time-updated set of tracks $\mathbb{I}_{t|t-1}$, and is characterized by

$$(w_{t|t-1}^i, n_{t|t-1}^i, p_{t|t-1}^i) = (w_{m_t^{\mathrm{b}}}, 1, q_{m_t^{\mathrm{b}}}), \tag{11}$$

where the scalar $0 \leq w_{m_t^{\mathrm{b}}} \leq 1$ denotes the credibility of the information reporting the entry.

3.2.3. Unidentified birth model

The "unidentified birth"' model m_t^{ub} accounts for the unidentified objects of interest that might have entered the scene since epoch $t-1$. By construction, the information on these potential objects is scarce. We shall represent them with a population of indistinguishable objects, with some p.d.f. $q_{m_t^{\mathrm{ub}}}$ collectively representing the state of each of these objects, an estimated size of $n_{m_t^{\mathrm{ub}}}$ objects, and some scalar $0 \leq w_{m_t^{\mathrm{ub}}} \leq 1$ representing the probability of existence of each object.

Recall from Assumption S.2 (in Section 3.1) that, for the sake of simplicity, the HISP filter collapses all the information on the unidentified objects in a single track. A single indistinguishable track $\mathrm{u}_{t|t-1} \in \mathbb{I}_{t|t-1}$ must aggregate the information on all the unidentified objects in the scene, i.e., those who have entered the scene through an unidentified birth, and have remained undetected in the scene ever since. More formally, it aggregates information on each of the indistinguishable tracks in the subset

$$\bigcup_{0 \leq t' \leq t} \bigcup_{m_{t'+1}^{\mathrm{e}} \in M_{t'+1}^{\mathrm{e}}} \cdots \bigcup_{m_t^{\mathrm{e}} \in M_t^{\mathrm{e}}} \left((m^{\psi}, \ldots, m^{\psi}, m_{t'}^{\mathrm{ub}}, m_{t'+1}^{\mathrm{e}}, \ldots m_t^{\mathrm{e}}), \boldsymbol{\phi}_{t-1}\right) \subseteq \bar{\mathbb{B}}_t \times \bar{\mathbb{O}}_{t-1} \tag{12}$$

As a convention, we set $\mathrm{u}_{t|t-1} = \left(m_{0:t}^{\mathrm{ub}}, \boldsymbol{\phi}_{t-1}\right) \in \bar{\mathbb{B}}_t \times \bar{\mathbb{O}}_{t-1}$, where $m_{0:t}^{\mathrm{ub}} = (m_0^{\mathrm{ub}}, \ldots, m_t^{\mathrm{ub}})$. The behavior history of the indistinguishable track does not reflect the pattern of any individual it represents; rather, it reflects the aggregated nature of the information it describes.

In the context of this paper, as it is often the case in SSA scenarios, very little information is available on the number or the spatial distribution of unidentified RSOs (i.e., not originating from a scheduled event) prior to their first detection by one of the sensors. There is little gain in propagating information on unidentified objects, and one can simply omit unidentified objects from past epochs and build the track $\mathrm{u}_{t|t-1}$ as

$$(w_{t|t-1}^{\mathrm{u}_{t|t-1}}, n_{t|t-1}^{\mathrm{u}_{t|t-1}}, p_{t|t-1}^{\mathrm{u}_{t|t-1}}) \approx (w_{m_t^{\mathrm{ub}}}, n_{m_t^{\mathrm{ub}}}, q_{m_t^{\mathrm{ub}}}). \tag{13}$$

If, on the other hand, the context necessitates to propagate information on unidentified objects, one can merge all the unidentified objects – whether newly-entered or pre-existing – into the indistinguishable track $\mathrm{u}_{t|t-1}$. The considered framework provides tools for the principled *merging* of sub-populations Houssineau (2015); Delande et al. (2016), and the merging procedure is described in Appendix A.1.

3.2.4. Time-updated tracks

The set of time-updated tracks $\mathbb{I}_{t|t-1}$ is formed with the distinguishable tracks $\mathbb{I}_{t-1} \setminus \{\mathrm{u}_{t-1}\}$ that have evolved in the scene since the previous epoch, those that have entered through a scheduled birth event, and the indistinguishable track representing the unidentified objects. More formally,

$$\begin{aligned}\mathbb{I}_{t|t-1} = \Big\{ & \big((\mathbf{b}_{t-1}, m_t^{\mathrm{e}}), \mathbf{o}_{t-1}\big) \\ & \text{s.t. } \big(\mathbf{b}_{t-1}, \mathbf{o}_{t-1}\big) \in \mathbb{I}_{t-1} \setminus \{\mathrm{u}_{t-1}\}, m_t^{\mathrm{e}} \in M_t^{\mathrm{e}} \Big\} \\ & \cup \bigcup_{m_t^{\mathrm{b}} \in M_t^{\mathrm{b}}} \big((\boldsymbol{m}_{t-1}^{\psi}, m_t^{\mathrm{b}}), \boldsymbol{\phi}_{t-1}\big) \cup \{\mathrm{u}_{t|t-1}\}. \end{aligned} \tag{14}$$

3.2.5. Computational complexity

Aside from identified birth events, we only consider behaviors that are not exclusive to an object and can thus be shared among tracks without restrictions. The time-update step is performed independently on each track, and has linear complexity with the number of tracks and evolution models. Algorithm 1, in Appendix B, illustrates the time-update step.

3.3. Data-update step

We now detail the data-update step of the HISP filter, at an arbitrary time step $t \in \mathbb{N}$ where a set of observations Z_t is collected from a data source. The source is assumed to be a finite-resolution sensor whose resolution cells (e.g., radar cells, pixels) are indexed by some set Z_t'; the collected observations $Z_t \subseteq Z_t'$ thus corresponds to the cells where a signal has been detected. It is further assumed that the operator possesses some knowledge on the data source, structured as follows:

- The detection, precision/accuracy are represented by a likelihood ℓ_t as in (7);
- The probability of a false positive in a cell $z \in Z_t$ is given by a scalar $0 \leq p_{t|t-1}^{\mathrm{fp}}(z) \leq 1$.

We shall consider a (possibly indistinguishable) time-updated track $i = (\mathbf{b}_t, \mathbf{o}_{t-1}) \in \mathbb{I}_{t|t-1}$, and a (possibly empty) observation $z \in \bar{Z}_t$. For the sake of convenience, we shall denote by $i:z$ the track resulting from their association, i.e., the data-updated track indexed by $(\mathbf{b}_t, (\mathbf{o}_{t-1}, z)) \in \bar{\mathbb{B}}_t \times \bar{\mathbb{O}}_t$, whose probability distribution $p_t^{i:z}$ is given by the data-update equation (6). The complexity of the data-update step lies, in fact, in the computation of the posterior weight $w_t^{i:z}$ assessing the credibility of the data-updated track $i:z$.

3.3.1. Association weight

The association between the predicted track i and the observation z is given by

$$\begin{aligned} \breve{w}_t^{i,z} &= w_{t|t-1}^i \int \ell_t(z|x) p_{t|t-1}^i(x) \mathrm{d}x \\ w_t^{i,z} &= \begin{cases} \breve{w}_t^{i,z}, & \text{if } z \in Z_t, \\ \breve{w}_t^{i,\phi} + (1 - w_{t|t-1}^i) & \text{if } z = \phi, \end{cases} \end{aligned} \tag{15}$$

where a higher *association weight* $w_t^{i,z}$ assesses track i as a likelier origin for observation z. Note that a track generating no observation is explained either by a missed detection ($\breve{w}_t^{i,\phi}$), or the non-existence of a potential object represented by the track ($1 - w_{t|t-1}^i$).

3.3.2. External weight

Following Assumptions **M**.1, **M**.2 (in Section 2.3), associations between objects and non-empty observations are exclusive. Given the association of track i with observation z, an *external weight* $w_{\mathrm{ex}}^{i,z}$ assesses the global matching between the remaining entities. A solution considering additional track-to-observation pairings, yet avoiding combinatorics, is conspicuously advantageous in large scale scenarios. The HISP filter relies on the assumption that

S.3 The origin object of any collected observation is moderately ambiguous, i.e., for any two distinct tracks $i, i' \in \mathbb{I}_{t|t-1}$ and any observation $z \in Z_t$, it holds that $w_t^{i,z} w_t^{i',z} \simeq 0$.

Assumption **S**.3 may appear vague and requires more explanation. Individual association weights (15) are assumed discriminating enough so that at most one track has significant association weight with any collected observation. In the construction of external weights, then, any additive term involving a product of the form $w_t^{i,z} w_t^{i',z}$ is considered negligible with respect to those that do not, and is discarded for the sake of simplicity Houssineau and Clark (2018). The

principled approximation S.3 is illustrated on the following example.

Example 2. *There are three distinguishable tracks i, j, k, no unidentified objects, and three collected observations z_1, z_2, z_3. To compute the posterior weight of track $i : z_1$, the global association between tracks j, k and observations z_2, z_3, ϕ is assessed. A natural construction of the external weight w_{ex}^{i,z_1} accounts for all possible pairings between the remaining entities:*

$$w_{\text{ex}}^{i,z_1} \propto \frac{w_t^{j,z_2}}{c(z_2)}\frac{w_t^{k,z_3}}{c(z_3)} + \frac{w_t^{j,z_2}}{c(z_2)}w_t^{k,\phi} + \frac{w_t^{j,z_3}}{c(z_3)}\frac{w_t^{k,z_2}}{c(z_2)} + \frac{w_t^{j,z_3}}{c(z_3)}w_t^{k,\phi} + w_t^{j,\phi}\frac{w_t^{k,z_2}}{c(z_2)} + w_t^{j,\phi}\frac{w_t^{k,z_3}}{c(z_3)} + w_t^{j,\phi}w_t^{z,\phi}, \tag{16}$$

where $c(z) = p_{t|t-1}^{\text{fp}}(z)/(1 - p_{t|t-1}^{\text{fp}}(z))$, for $z = z_2, z_3$. The combinatorial nature of the expression (16) is clearly visible, but we can rewrite it as

$$\begin{aligned} w_{\text{ex}}^{i,z_1} &\propto \left[w_t^{j,\emptyset} + \frac{w_t^{j,z_2}}{c(z_2)} + \frac{w_t^{j,z_3}}{c(z_3)}\right]\left[w_t^{k,\emptyset} + \frac{w_t^{k,z_2}}{c(z_2)} + \frac{w_t^{k,z_3}}{c(z_3)}\right] \\ &\quad - \frac{w_t^{j,z_2}}{c(z_2)}\frac{w_t^{k,z_2}}{c(z_2)} - \frac{w_t^{j,z_3}}{c(z_3)}\frac{w_t^{k,z_3}}{c(z_3)} \\ &\simeq \left[w_t^{j,\emptyset} + \frac{w_t^{j,z_2}}{c(z_2)} + \frac{w_t^{j,z_3}}{c(z_3)}\right]\left[w_t^{k,\emptyset} + \frac{w_t^{k,z_2}}{c(z_2)} + \frac{w_t^{k,z_3}}{c(z_3)}\right], \end{aligned} \tag{17}$$

where the approximation follows from Assumption S.3. The approximated weight (17) amounts to a product of track-specific terms, each involving a sum over observation-specific terms: its computational complexity is thus linear in the number of tracks and observations.

In the general case, the external weight $w_{\text{ex}}^{i,z}$ is computed by the HISP filter as

$$w_{\text{ex}}^{i,z} = C_t(i,z) \prod_{i' \in \mathbb{I}_{t|t-1} \setminus \{\mathrm{u}_{t|t-1}, i\}} \left[w_t^{i',\phi} + \sum_{z' \in Z_t \setminus \{z\}} \frac{w_t^{i',z'}}{c_t(z')}\right], \tag{18}$$

where

$$\begin{aligned} c_t(z') &= \frac{w_t^{\mathrm{u}_{t|t-1},z'}}{w_t^{\mathrm{u}_{t|t-1},\phi}} + \frac{p_{t|t-1}^{\text{fp}}(z')}{1 - p_{t|t-1}^{\text{fp}}(z')}, \\ C_t(i,z) &\propto \left[w_t^{\mathrm{u}_{t|t-1},\phi}\right]^{-\mathbf{1}_{\mathrm{u}_{t|t-1}}(i)} \prod_{z' \in Z_t \setminus \{z\}} c_t(z'). \end{aligned} \tag{19}$$

As shown by the expressions (18), (19), Assumption S.3 breaks the combinatorial complexity of global association terms into a more manageable complexity, linear with the number of tracks and observations. Due to its nature, this assumption holds well in scenarios where the distance between objects is typically larger than the sensors' resolution scale, which appears reasonable in the context of SSA. Note that the constant of proportionality in (19) does not have to be explicitly given: as it will be seen in the expression of the posterior weights (20), only the ratios of external weights need to be computed.

3.3.3. Posterior weight

The posterior weight $w_t^{i:z}$ is then equivalently given by

$$w_t^{i:z} = \frac{w_{\text{ex}}^{i,z}\breve{w}_t^{i,z}}{\sum_{i' \in \mathbb{I}_{t|t-1}} w_{\text{ex}}^{i',z} w_t^{i',z}} \left(= \frac{w_{\text{ex}}^{i,z}\breve{w}_t^{i,z}}{\sum_{z' \in \bar{Z}_t} w_{\text{ex}}^{i,z'} w_t^{i,z'}}\right), \tag{20}$$

where the association and external weights are given by (15) and (18), respectively.

3.3.4. Data-updated tracks

The set of data-updated tracks $\mathbb{I}_t$ is formed with all the associations between the time-updated tracks $\mathbb{I}_{t|t-1}$ and the observations Z_t, or the empty one ϕ. More formally,

$$\mathbb{I}_t = \left\{\left(\mathbf{b}_t, (\mathbf{o}_{t-1}, z)\right) \text{ s.t. } \left(\mathbf{b}_t, \mathbf{o}_{t-1}\right) \in \mathbb{I}_{t|t-1}, z \in \bar{Z}_t\right\}. \tag{21}$$

It includes in particular new distinguishable tracks of the form $\left(m_{0:t}^{\text{ub}}, (\boldsymbol{\phi}_{t-1}, z)\right)$, $z \in Z_t$, corresponding to an object that entered the scene at an unknown epoch but has just been identified through its first detection.

3.3.5. False positives

As it will be seen in Section 3.4, it is also of interest to compute the *posterior* probability that an observation $z \in Z_t$ is a false positive for the sole purpose of track extraction. A false positive can be seen as the detection of a transient "track" that only exists at that particular time t. The computation of the posterior probability of false positive $p_t^{\text{fp}}(z)$ then amounts to the computation of a posterior weight, following filtering equations almost identical to the expressions (18), (20). More precisely, the external

weight $w_{\text{ex}}^{\text{fp},z}$ is given by

$$w_{\text{ex}}^{\text{fp},z} = C_t(\text{fp}, z) \prod_{i \in \mathbb{I}_{t|t-1} \setminus \{\text{u}_{t|t-1}\}} \left[w_t^{i,\phi} + \sum_{z' \in Z_t \setminus \{z\}} \frac{w_t^{i,z'}}{c_t(z')} \right], \tag{22}$$

where

$$C_t(\text{fp}, z) \propto \left[1 - p_{t|t-1}^{\text{fp}}(z)\right]^{-1} \prod_{z' \in Z_t \setminus \{z\}} c_t(z'). \tag{23}$$

The posterior probability of a false positive in $z \in Z_t$ is then given by

$$p_t^{\text{fp}}(z) = \frac{w_{\text{ex}}^{\text{fp},z} p_{t|t-1}^{\text{fp}}(z)}{\sum_{i \in \mathbb{I}_{t|t-1}} w_{\text{ex}}^{i,z} w_t^{i,z} + w_{\text{ex}}^{\text{fp},z} p_{t|t-1}^{\text{fp}}(z)}. \tag{24}$$

We can uniquely identify this false-positive track, at any time $t' \geq t$, with the track index $i = \left(\boldsymbol{m}_{t'}^{\psi}, (\phi, \ldots, \phi, z, \phi, \ldots, \phi)\right) \in \bar{\mathbb{B}}_{t'} \times \bar{\mathbb{O}}_{t'}$, with posterior weight $w_{t'}^i = p_t^{\text{fp}}(z)$, and we denote by $\mathbb{I}_{t'}^{\text{fp}}$ the set of all false-positive tracks up to time t'.

3.3.6. Computational complexity

The computation of the posterior probability distributions are performed independently for each track-to-observation association. The complexity of the data-update step reduces to the complexity of the computation of the posterior weights, linear with the number of tracks and observations. Algorithm 2, in Appendix B, illustrates the data-update step.

3.4. Track extraction

While the HISP filter marginalizes the probabilities of existence over each track, Assumption M.2 (in Section 2.3) implies that the observation-to-object associations are exclusive and the existence of tracks are interdependent. This must be accounted for when a population estimate is to be extracted from the filter's output.[7]

A population estimate can then be formed with the subset of tracks that are the likeliest *and* that explain all the observations collected so far, i.e., the subset

$$I_t^* = \underset{I \subseteq \mathbb{I}_t \cup \mathbb{I}_t^{\text{d}} \cup \mathbb{I}_t^{\text{fp}}}{\text{argmax}} \sum_{i \in I} \log w_t^i \ \text{ s.t.}$$
$$\forall z \in Z_{t'},\ 0 \leq t' \leq t,\ \exists!(\mathbf{b}, \mathbf{o}) \in I,\ [\mathbf{o}]_{t'} = z, \tag{25}$$

where "$\exists!$" stands for "there is a unique", and $[\mathbf{o}]_{t'}$ denotes the t'-th element in the observation history $\mathbf{o}$. That is, each collected observation must appear once and only once in the combined observation histories of the selected tracks I_t^*. By construction, $I_t^* \cap \mathbb{I}_t$ represents the population of objects that are still in the scene, $I_t^* \cap \mathbb{I}_t^{\text{d}}$ those that have left the scene at some point in the past, and $I_t^* \cap \mathbb{I}_t^{\text{fp}}$ the false positives. For most practical purposes, only the former subset is of interest to the operator.

Note that the complexity of the track extraction step (25) is not linear with the number of tracks or observations, though it is a standard optimization problem that can be solved through integer programming. There is a wealth of well-established linear/integer programming libraries available online that are optimized specifically for that purpose; we used, for instance, the GNU Linear Programming Kit (GLPK)®. Note also that the track extraction process is independent from the filtering process; it does not have to be performed at each time step, and can be performed offline on a separate computing unit whenever one wishes to update the population estimate for operational purposes.

In scenarios where the measurement ambiguity is moderate at most one track, among tentative ones sharing non-empty observations, is likely to be confirmed throughout the filtering process. For the sake of computational efficiency, then, the constraint in the optimization problem (25) can be evaluated on a sliding window $\{t - \Delta_{\text{e}}, \ldots, t\}$ rather the full time histories, that is, the tracks that have been observed at least once in the sliding window are selected through the optimization problem

$$\underset{I \subseteq \mathbb{I}_t \cup \mathbb{I}_t^{\text{d}} \cup \mathbb{I}_t^{\text{fp}}}{\text{argmax}} \sum_{i \in I} \log w_t^i \ \text{ s.t. } \ \forall z \in Z_{t'},$$
$$\max(0, t - \Delta_{\text{e}}) \leq t' \leq t, \exists!(\mathbf{b}, \mathbf{o}) \in I,\ [\mathbf{o}]_{t'} = z, \tag{26}$$

while the remaining tracks are selected on an individual basis, i.e., if their posterior weight exceeds some threshold τ_{e} fixed by the operator. A longer sliding window reduces the possibility of extracting conflicting tracks to the expense of computational cost.

[7] Note that tracks cannot exist simultaneously either if they originate from the same identified birth, since it relates to a single individual. We have not integrated that additional constraint in the current track extraction procedure, but it will be added in subsequent versions of the algorithm.

3.5. Approximations for efficient computation

We present a few options in order to reduce the computational cost of the HISP filter.

3.5.1. Pruning tracks

Pruning tracks with negligible weight is a common feature in multi-target filters. A simple solution is to discard from the stochastic population $\{w_t^i, n_t^i, p_t^i\}_{i\in\mathbb{I}_t}$ the tracks whose probability of existence falls below some threshold τ_p fixed by the operator.

3.5.2. Merging probability distributions

In the context of SSA, as it will be apparent in the numerical studies presented in Section 4, the time-update equation (5) is the most computationally demanding operation of the HISP filter when it relies on a high-fidelity orbital propagator. If a subset of distinct tracks have "close" distributions in the sense of some appropriate metric, there is little gain in maintaining distinct information on their individual states.[8] One option is to maintain a common probability distribution describing each of these "close" tracks, in order to spare unnecessary time-update and data-update operations on their individual probability distributions. A more formal description of the merging procedure is given in Appendix A.2.

Note that the tracks sharing a common probability distribution still maintain their individual index, behavior and observation histories, and weight for the purpose of filtering and track extraction. The filter maintains the same information on their state, but they remain *distinguishable* from one another for the purpose of estimation.

3.5.3. Merging tracks

If the track extraction procedure is implemented over a sliding window $\{t-\Delta_\mathrm{e}, \ldots, t\}$, as shown in (26), then an additional merging procedure can be proposed. If some tracks already share the same probability distribution (under the procedure described above), and have identical behavior and observation histories over the sliding window as well, they are likely to describe the same object in the population. By construction, they are also highly unlikely to be concurrently extracted, and thus the stochastic population (8) maintained by the HISP filter can be simplified by merging these tracks into a single one.

Since the candidate tracks are assumed to be distinct representations of the same object, the weight of the merged track is set as the sum of the individual weights of the candidate tracks[9]. In order for the merged track to be well-defined, its index must be part of the set of indices $\bar{\mathbb{B}}_t \times \bar{\mathbb{O}}_t$. A natural and straightforward solution is to transfer the behavior/observation history of the candidate track with the highest weight to the merged track.

4. The HISP filter: implementation for a SSA scenario

We illustrate the HISP filter on a SSA scenario, described in Section 4.1. Our Sequential Monte Carlo (SMC) implementation of the HISP filter is briefly covered in Section 4.2, and simulation results are discussed in Section 4.3.

4.1. Scenario implementation

The scenario focuses on the near-Earth space and the estimation of the RSOs' kinematic state: the object state space $\mathbf{X} \subseteq \mathbb{R}^6$ describes the Cartesian coordinates (position and velocity) in the J2000 Earth-Centered Inertial (ECI) frame. Exploiting GPS data transmitted by PlanetLabs, LEO trajectories for 115 satellites of the Dove constellation were produced through a batch-least-square method, for a period covering the most part of March 5, 2018 (see Figure 1). The scenario lasts 23 h20 min, discretized in 700 time steps of 120 s each. The ground truth data is built with one data point per satellite and per time step. The 115 satellites are labeled arbitrarily. When the scenario starts, at time $t = 0$, the satellites with indices 1 to 104 are already in the near-Earth space unbeknown to the operator; their existence, as well as their initial state, is to be inferred through the collected observations. At time $t = 49$ (respectively (resp.) $t = 99$), the satellites with indices 105 to 110 (resp. 111 to 115) appear in the scene through individual scheduled events. The initial state of a satellite entering the scene through a scheduled event is transmitted to the operator, but it is corrupted beforehand with an additive Gaussian noise, with zero mean and covariance matrix Q^b, diagonal

[8] For example, when two tentative tracks differ only on a few elements in their observation histories, and are likely to represent the same object of interest.

[9] Note that if the resulting sum exceeds one, all the candidate tracks cannot be the representatives of the same object, and thus the merging operation should be stopped. In practical cases, however, we have not yet encountered this situation.

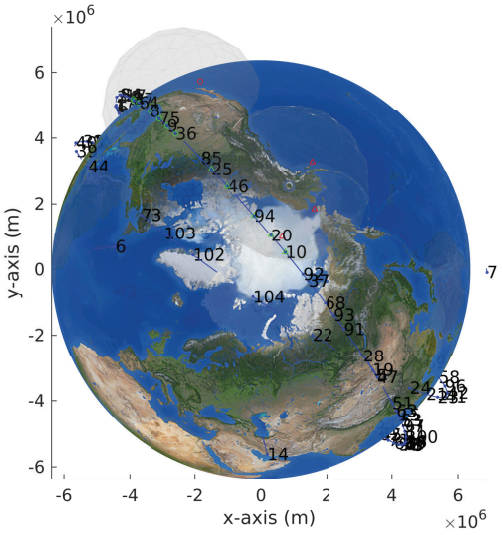

Figure 1: Scenario illustration. Satellites are depicted by labeled points, sensor FoVs by gray volumes, false positives by red dots, and true observations by green dots.

with a standard deviation of 10 m on the position coordinates, and $1\,\mathrm{m\,s^{-1}}$ on the velocity coordinates.

The sensor data is generated from two simulated radars with Doppler effect, sharing the same characteristics and located in Midland, TX and Fairbanks, AL.[10] The observation space $\mathbf{Z}_t \subseteq \mathbb{R}^4$ describes the range ρ, angles θ, φ, and range rate $\dot{\rho}$ components in the sensor's local topocentric frame. Observations are collected at each time step; each RSO lying within the FoVs is detected with a probability of $p_{\mathrm{d},t} = 0.98$, assumed constant and uniform across the FoV. False positives are uniformly distributed in the FoV, and their number is Poisson distributed with an average of 1 false positive per sensor and per scan. The FoV, sensor resolution, and noise characteristics are described in Table 1.

The FoV of each sensor, in the position subspace, is illustrated by the gray area in Figure 1. For the sake of simplicity, we assume that the data collection dates of both sensors are synchronized with the time flow, i.e., two successive data steps are performed at each time step to process the observations of the two sensors.

[10] These correspond to the location of two stations in Leolabs, Inc.'s radar network.

Table 1: Sensor resolution, noise characteristics, and field of view.

	Cell resolution/ Noise (std. dev.)	Field of view
Range ρ (km)	0.1	$[10 \quad 2500]$
Azimuth θ (°)	0.1	$[-90 \quad 90]$
Elevation φ (°)	0.1	$[-90 \quad 90]$
Range rate $\dot{\rho}$ ($\mathrm{m\,s^{-1}}$)	10	$[-1\times10^4 \quad 1\times10^4]$

4.2. Filter implementation

We provide a brief description of our SMC implementation of the HISP filter for SSA Delande et al. (2017, 2018a,c). A more detailed description is given in Appendix C.

4.2.1. Probability distributions for orbiting objects

Due to the peculiar nature of uncertainty regions for orbiting objects, we adopt a non-parameterized representation of the single-object probability distributions, maintained with sets of weighted particles Doucet et al. (2001). The probability distribution of each track in $\mathbb{I}_t$ is approximated by a set of 100 weighted particles.

4.2.2. Time-update step

We consider only one evolution model m_t^{e} corresponding to a stable, LEO trajectory. Our earlier implementation of the HISP filter adopted a simple, unperturbed model with additive noise Delande et al. (2017) that proved too coarse and inaccurate for a scenario based on real trajectories.We developed a faithful orbital prediction model for a single target tracking problem in Delande et al. (2018c), and we adopt it here. The modeled perturbations include the zonal/tesseral effects of the Earth's gravitational field up to order and degree 20, the gravitational pull of the Sun and the Moon, the solar radiation pressure (for an AMR of $0.0015\,\mathrm{m^2\,kg^{-1}}$, and a spherical shape with a radiation pressure coefficient of 0.3), and a drag term based on the MSIS86 atmospheric model (for a ballistic coefficient of $25\,\mathrm{kg\,m^{-2}}$). Non-modeled perturbations are accounted for with a zero-mean Gaussian noise with standard deviation $10^{-6}\,\mathrm{m\,s^{-3}}$ on each component in the object's Radial-Intrack-Crosstrack (RIC) frame. Since the evolution model describes a stable trajectory, the probability for an object to stay in the scene is set to $p_{m_t^{\mathrm{e}}} = 1 - 10^{-10}$. In practice, tracks that have left the scene have negligible weights and are discarded through pruning.

Birth events are scheduled a times $t = 49$ and $t = 99$, as discussed in Section 4.1. Each identified birth model $m_t^{\mathrm{b}} \in M_t^{\mathrm{b}}$ is described in (11) with a Gaussian distribution $q_{m_t^{\mathrm{b}}}$ on $\mathbf{X}$, whose mean is the satellite's true initial state corrupted with noise and whose covariance is the noise covariance matrix Q^{b}. The weight $w_{m_t^{\mathrm{b}}}$ of each birth model is set to one, that is, the operator has full confidence in the occurrence of the reported births.

Unidentified births act as "pool" from which individuals can be drawn to explain the collected observations. Up to one unidentified birth could occur per resolution cell, the population size in (13) is thus set to $n_{m_t^{\mathrm{ub}}} = 2|Z'_t|$, where the number of cells $|Z'_t|$ denotes the volume of each sensor FoV. The unidentified births are assumed uniformly distributed across the sensor FoVs. The operator has no information on the population of RSOs already in the scene at $t = 0$, but they expect an average of 100 unidentified objects to be detected for the first time throughout a day (720 steps), so that the predicted weight is set to $w_{m_t^{\mathrm{ub}}} = 100/(720 * 2|Z'_t|)$.

4.2.3. Data-update step

Instead of representing the radar's observation process with a *random* variable, we exploit a more general representation of an uncertain phenomenon through *uncertain* variables Houssineau (2018); Houssineau and Bishop (2018). The *epistemic* uncertainty, reflecting an observer's limited knowledge on the phenomenon, is distinguished from the *aleatory* uncertainty characterizing the phenomenon's inherent randomness – if any. This alternative representation is convenient to model uncertain components on which information is scarce. It has been exploited to represent USStratCom' TLEs in a single-RSO Bayesian tracking problem Delande et al. (2018c), and then to represent the RSO's state and its orbital propagation model, as well Delande et al. (2018b). The construction of the potential g_t in (7), describing the precision/accuracy of the radar, is detailed in Appendix C.

Since no prior information is assumed on the spatial distribution of unidentified objects, the posterior p.d.f. of a newborn track is initialized through the admissible region approach developed in DeMars and Jah (2013).

4.2.4. Track extraction

While the track extraction presented in Section 3.4 is not part of the filtering process and one does not need to extract a population estimate at each time step, we do so in order to compare the filter's output with the ground truth. A trade-off between computational efficiency and quality of estimation is set with a sliding window of $\Delta_e = 6$, and a weight threshold of $\tau_{\mathrm{e}} = 0.7$. That is, the tracks that have not been observed in the last 6 time steps are extracted, on an individual basis, if their probability of existence exceeds 70%. Then, the subset of remaining tracks that most likely explains all the observations collected in the last 6 time steps is jointly extracted through the maximization problem (26).

4.2.5. Approximations

The pruning threshold is set at $\tau_{\mathrm{p}} = 10^{-4}$, a significantly lower value than the extraction threshold τ_{e}. The pruned tracks are, therefore, extremely unlikely candidates for the extraction process and pruning them do not affect the quality of the estimated population.

Merging probability distributions of individual tracks proves to be challenging. Since the object state space $\mathbf{X}$ describes the Cartesian coordinates in the J2000 ECI frame, defining a metric d_{m} between two probability distributions on $\mathbf{X}$ and a threshold τ_m reflecting the "closeness" of orbital trajectories makes little physical sense. We propose instead to perform the merging in an alternative space equipped with spherical coordinates where the distributions can be approximated as Gaussian (see Appendix C for more details). In order to limit merging opportunities and mitigate information loss, the merging threshold τ_{m} is set as the 5%-confidence region for a chi-square distribution with 6 degrees of freedom, i.e., $\tau_{\mathrm{m}} \approx 1.63$.

In addition to the merging of probability distributions, tracks are merged with a similar[11] method as explained in Section 3.5.

4.3. Numerical results

At any time $t \in \mathbb{N}$ we compare the extracted tracks that are still in the scene, i.e., those indexed by $I_t^* \cap \mathbb{I}_t$ (see Section 3.4), with the ground truth built from PlanetLabs' GPS data.

4.3.1. Methodology

A correspondence between the extracted tracks $I_t^* \cap \mathbb{I}_t$ and the constellation of Planetlabs is estab-

[11] The results presented in this paper are based on a slightly different version of the merging procedure that only compares the observation histories of the tracks, rather than their full behavior/observation histories.

lished in order to produce individual statistics for each satellite. If a track originates from an identified birth, it is naturally associated to the satellite launched through this birth event. If the track originates from an unidentified birth, the association depends on the first observation in the track's history. If it is a false positive, the track is considered a "false track", otherwise, the track is associated to the satellite that produced the observation.

The version of the HISP filter exploited in this paper does not propagate information on the unidentified, yet-to-be-detected objects (see Section 4.2). The population estimate is thus compared to the *identifiable* RSOs, i.e., those that have entered the scene through an identified birth and/or have been detected at least once.

The results are averaged over 100 Monte Carlo (MC) runs, across which the ground truth and the scheduled births are identical but the observations generated from the two simulated radars vary. Since the time of first detection of a RSO may vary across MC runs, it is considered *identifiable* if has entered the scene through an identified birth and/or if it has entered a sensor FoV at least once.

The algorithm was coded in object-oriented C++®, and run on a single 2.1GHz Intel Xeon Platinum® 8160 node of the Texas Advanced Computing Center (TACC).

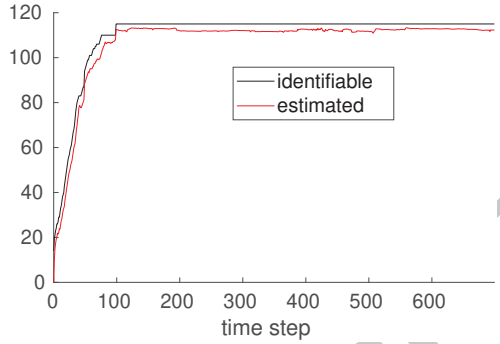

(a) Number of objects

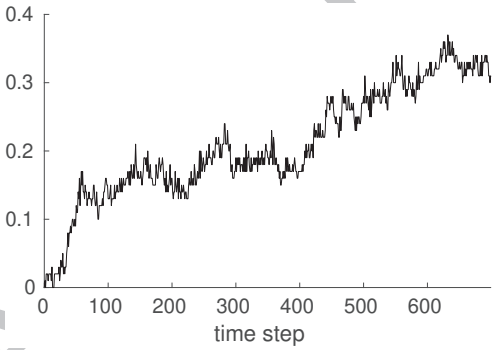

(b) Number of false tracks

Figure 2: Global statistics (on 100 MC runs)

4.3.2. Global statistics

The number of identifiable satellites is compared with the number extracted tracks, excluding the false tracks, and the results are depicted in Figure 2a. We see that the HISP maintains a reasonably accurate estimation of the population size, given the poor sensor coverage and the limited number of scheduled birth events (only 11, out of 115 satellites). The number of false tracks remains limited throughout the scenario, as shown in Figure 2b.

The four plots in Figure 3 show the run time of the HISP filter, across the four operations performed at each time step. The linear complexity of the time- and data-update filtering steps with the number of tracks is clearly visible. The origin of the spike in run time computation around time step 500 is unclear; it may be due to an unusual number of satellites in the sensor FoVs, inducing an unusual number of collected observations and thus a large number of data-updated tracks. Unsurprisingly, the orbital propagation through numerical integration is particularly time-consuming and most of the computational effort is spent on the time-update step.

4.3.3. Individual statistics

Individual statistics are also produced for each satellite, as in Figure 4. The number of extracted tracks (Figure 4a) indicates whether the satellite is correctly represented by a single track in the population estimate, or misrepresented (either with no track, or with more than one). If several tracks are extracted for the same satellite, the one with the smallest Root Mean Square Error (RMSE) on the position components is considered the best track. The RMSE of the best track on the position and velocity components (Figures 4c, 4d), provide a measure of the track quality. The number of track swaps (Figure 4b) assesses the ability of the filter to maintain track custody. A track swap occurs when the best track extracted at some time step t does not originate from the best track extracted at the previous time step $t-1$; that is, when the filter switches to a different behavior/observation history to describe the satellite. General patterns can be discerned among the individual statistics obtained for the 115 satellites; for the sake of clarity, the individuals statistics are categorized in a few relevant profiles presented in

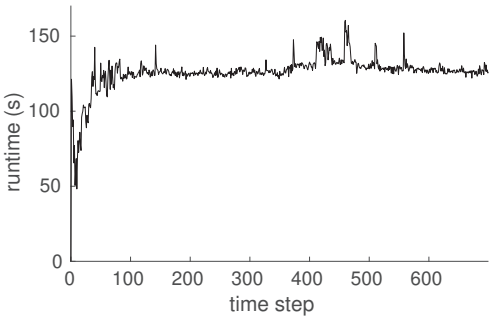

(a) Runtime (time-update)

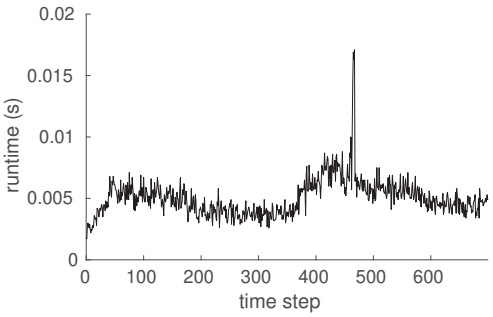

(b) Runtime (data-update)

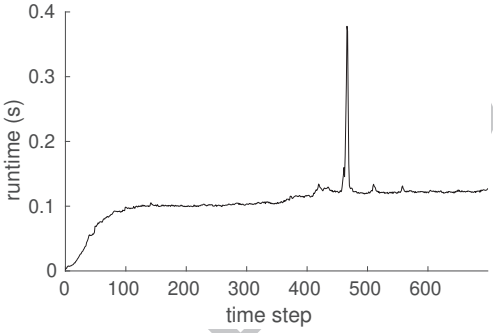

(c) Runtime (approximation)

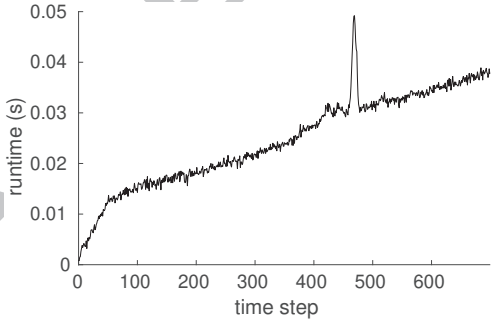

(d) Runtime (track extraction)

Figure 3: Global statistics (on 100 MC runs) (cont.)

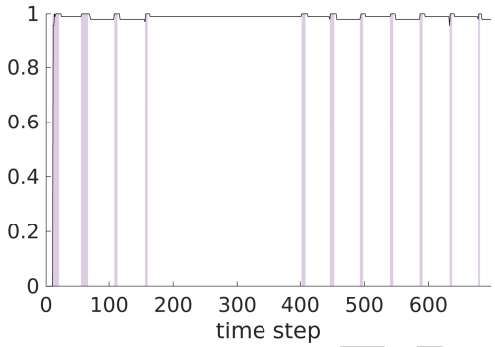

(a) Number of tracks

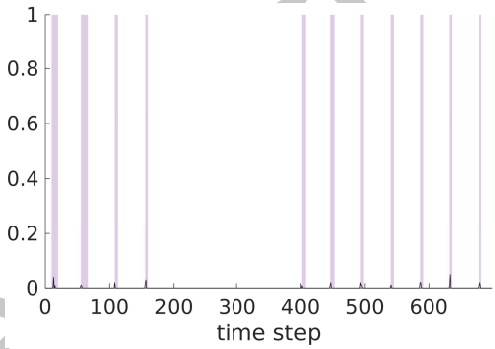

(b) Number of track swaps

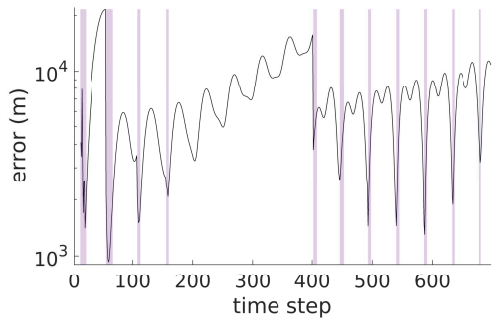

(c) RMSE of best track (position)

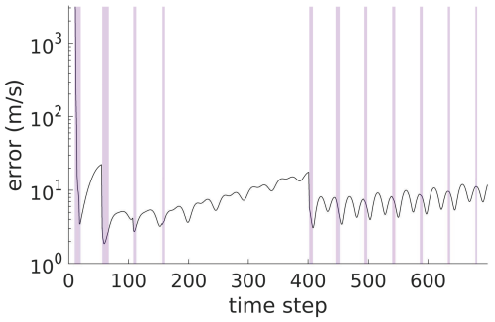

(d) RMSE of best track (velocity)

Figure 4: Statistics for satellite 36 (on 100 MC runs). The blue bars denote sensor coverage.

the following paragraphs.

A profile representative of 60 objects is depicted in Figure 4, in which the satellite is detected at its first entry in a sensor FoV and the track custody is well maintained over the scenario. Note that the uncertainty in the satellite's state increases significantly outside observation windows, notably in the position subspace. This is due to the significant process noise accounting for the limited fidelity of the orbital propagation model. This trend is widespread among the individual statistics, and more pronounced for satellites identified through a birth event where the initial, concentrated distribution quickly spreads through orbital propagation (see Figure 5).

A profile representative of 19 objects is depicted in Figure 6, in which the detection of the satellite does not always occur at is first entry (or, if it is, the initial track is rapidly discarded). The track-per-satellite ratio shows that, in the case, the filter consistently fails at maintaining track custody throughout the first pass in a sensor FoV.

A profile representative of 22 objects is depicted in Figure 7, in which track custody is lost and reacquired almost immediately, usually following re-entry in a sensor FoV. It is likely due to a significant mismatch between the track and the observations at re-entry, so that the filter discards the old track for a new one explaining the recent observations. A similar profile, representative of 3 objects, is depicted in Figure 8; the track is not reacquired before the next re-entry in a sensor FoV. These previous cases suggest that the process noise does not (always) account for the bias in the orbital model. A profile representative of 2 objects is depicted in Figure 9, in which the track-per-satellite ratio and the low number of track swaps suggest that filter maintains track custody in some runs, but performs poorly on others where observations are perhaps too scarce. A profile representative of 2 objects is depicted in Figure 10, in which the satellite is mistakenly represented by several tracks on a significant number of runs. This unusual situation suggests that tracks are competing for the observations produced from the same satellite, while maintaining high weights warranting their extraction. The reason for this behavior, at this stage in the analysis, is unclear. Finally, a profile representative of 7 objects is depicted in Figure 11, in which the HISP filter fails at maintaining track custody in a significant number of runs, resulting into frequent track swaps and inconsistent performance statistics.

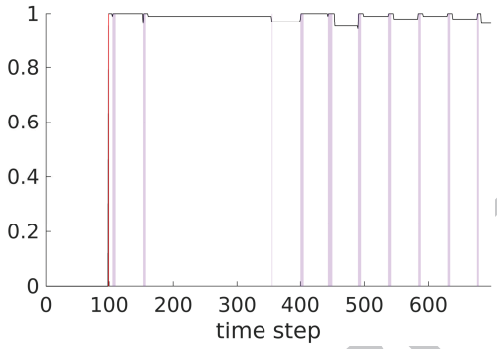

(a) Number of tracks

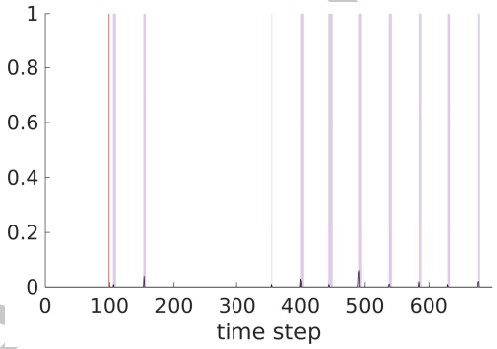

(b) Number of track swaps

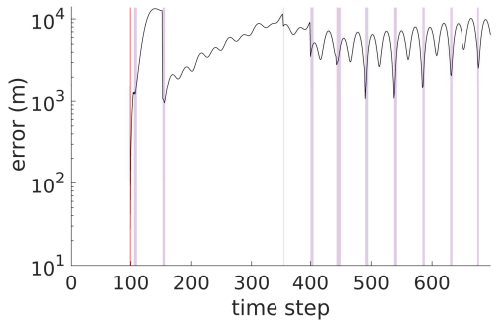

(c) RMSE of best track (position)

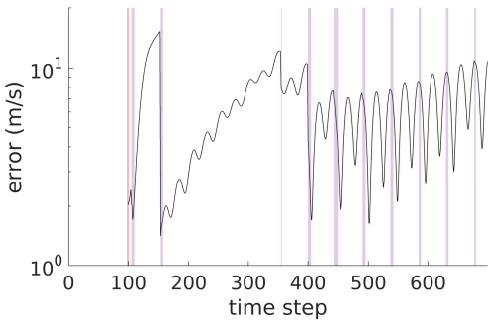

(d) RMSE of best track (velocity)

Figure 5: Statistics for satellite 114 (on 100 MC runs). The red line indicates the scheduled birth event, the blue bars denote sensor coverage.

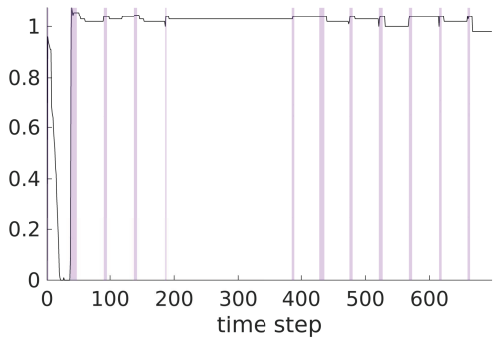

(a) Number of tracks

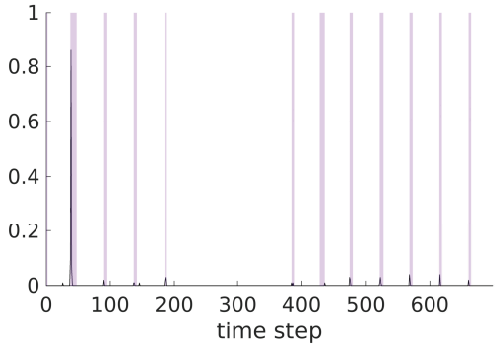

(b) Number of track swaps

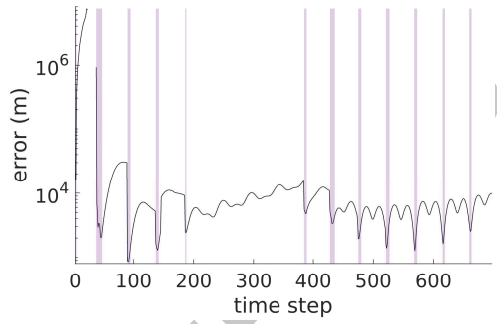

(c) RMSE of best track (position)

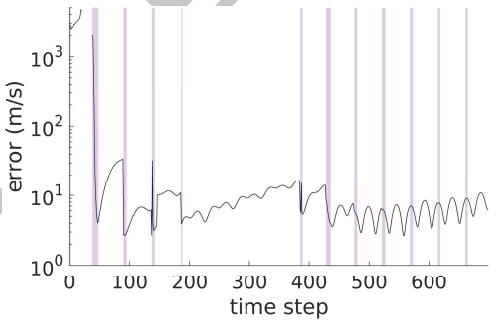

(d) RMSE of best track (velocity)

Figure 6: Statistics for satellite 78 (on 100 MC runs). The blue bars denote sensor coverage.

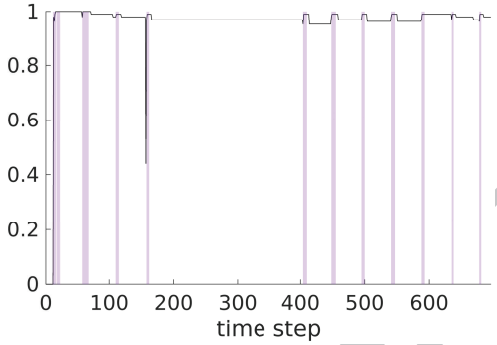

(a) Number of tracks

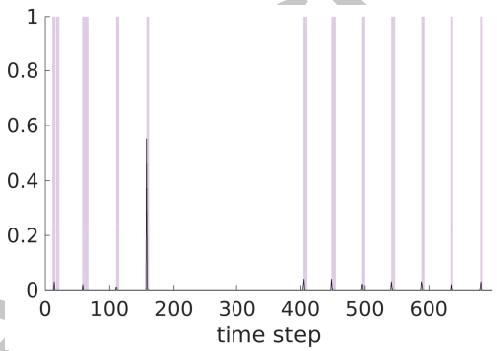

(b) Number of track swaps

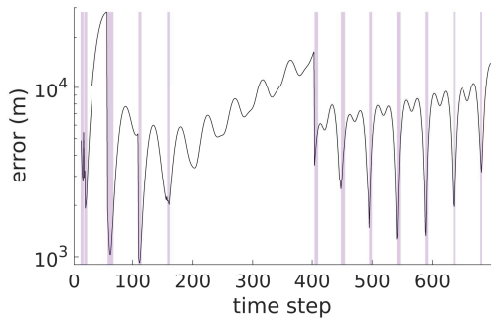

(c) RMSE of best track (position)

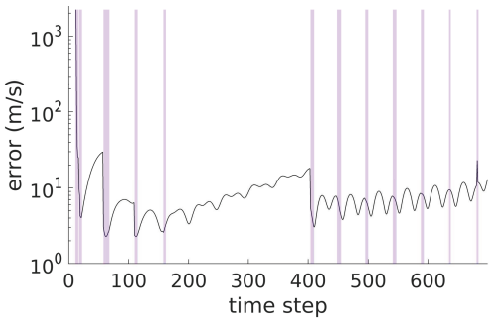

(d) RMSE of best track (velocity)

Figure 7: Statistics for satellite 8 (on 100 MC runs). The blue bars denote sensor coverage.

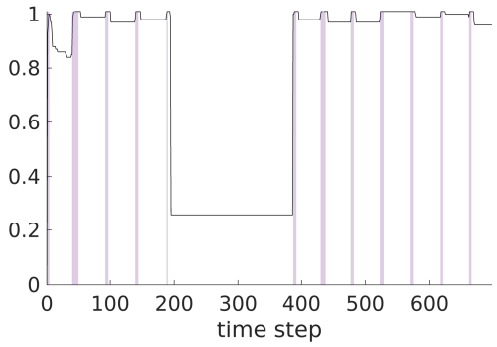

(a) Number of tracks

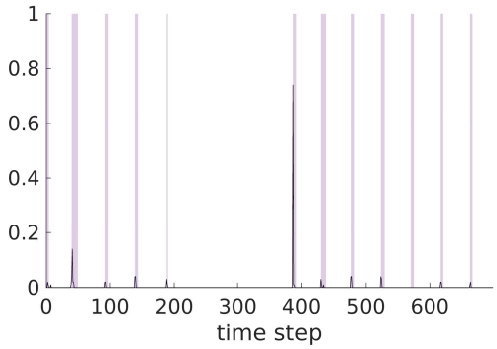

(b) Number of track swaps

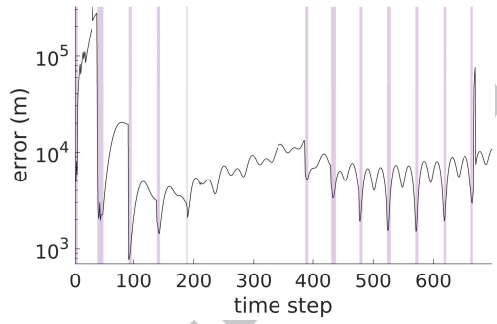

(c) RMSE of best track (position)

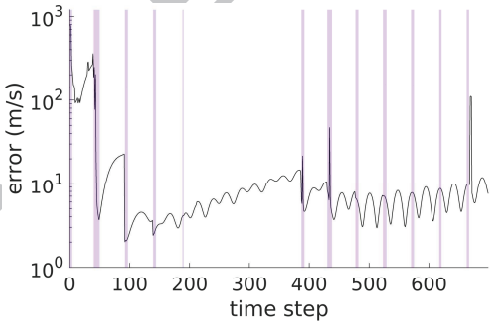

(d) RMSE of best track (velocity)

Figure 8: Statistics for satellite 100 (on 100 MC runs). The blue bars denote sensor coverage.

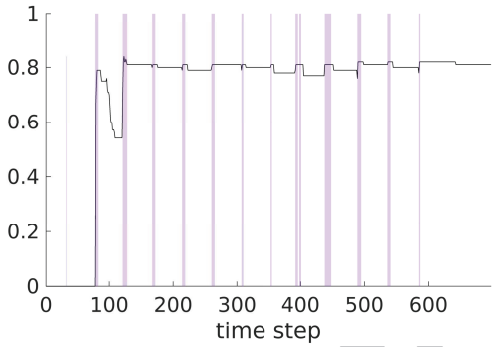

(a) Number of tracks

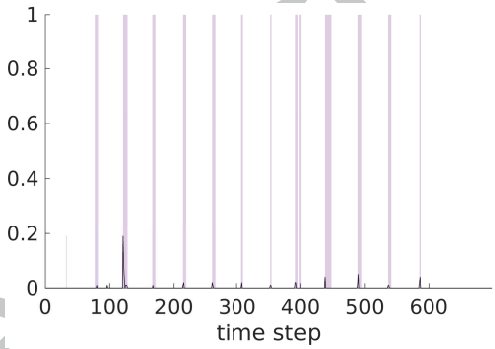

(b) Number of track swaps

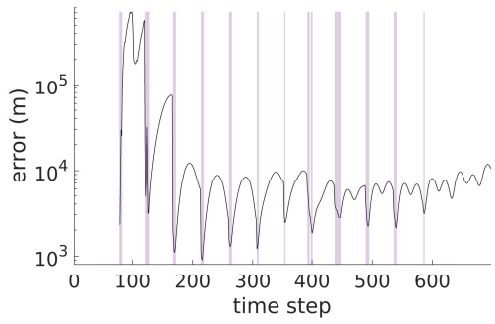

(c) RMSE of best track (position)

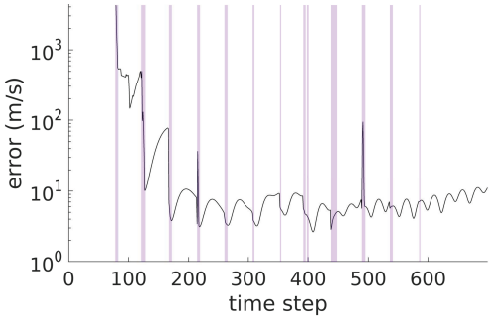

(d) RMSE of best track (velocity)

Figure 9: Statistics for satellite 42 (on 100 MC runs). The blue bars denote sensor coverage.

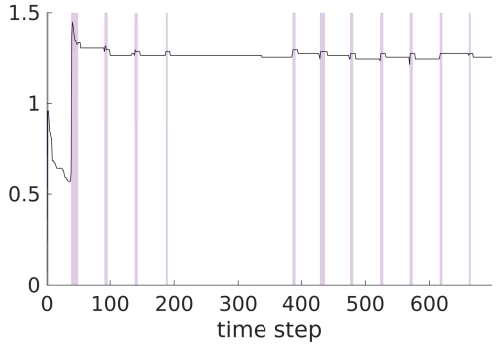

(a) Number of tracks

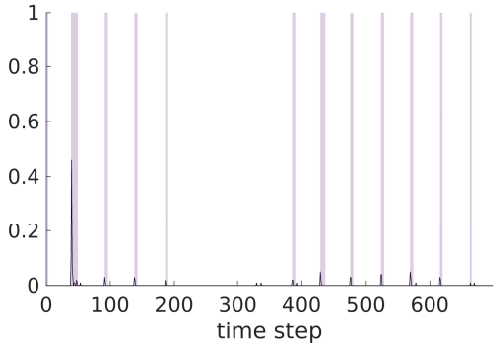

(b) Number of track swaps

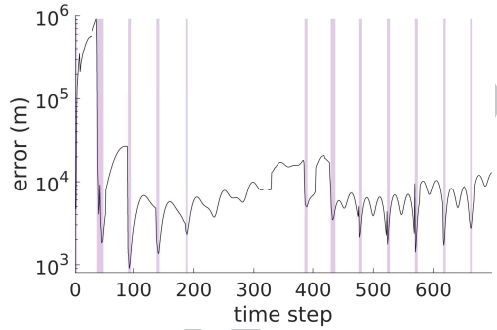

(c) RMSE of best track (position)

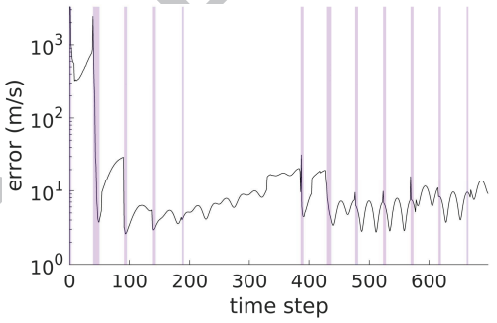

(d) RMSE of best track (velocity)

Figure 10: Statistics for satellite 86 (on 100 MC runs). The blue bars denote sensor coverage.

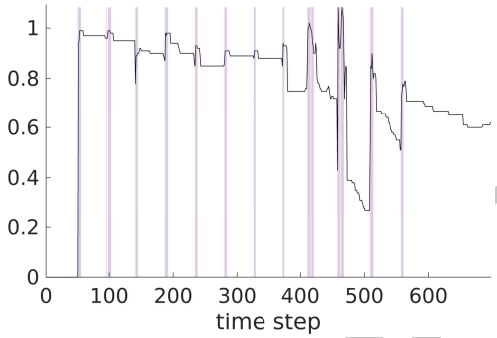

(a) Number of tracks

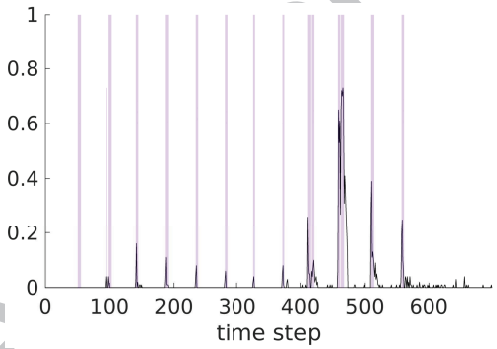

(b) Number of track swaps

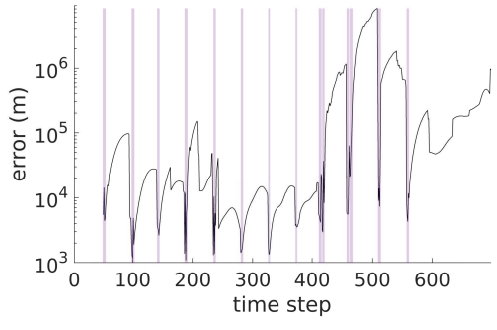

(c) RMSE of best track (position)

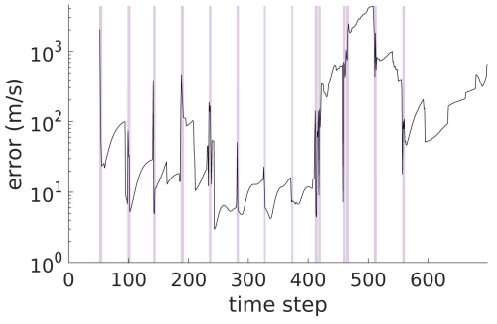

(d) RMSE of best track (velocity)

Figure 11: Statistics for satellite 35 (on 100 MC runs). The blue bars denote sensor coverage.

4.3.4. Discussion

Overall, the HISP filter shows good tracking performances on this challenging scenario. The running time of the algorithm confirms the linear complexity of the time- and data-update steps with the number of RSOs. The scalability of the HISP filter to a large-scale scenarios is a promising feature for the construction of large catalogue of RSOs. Its computational efficiency largely depends on the implementation of the single-object filtering mechanisms; since the time- and data-update steps are performed on individual probability distributions independently from one another, a parallel implementation of the algorithm should improve it significantly.

Similarly to most multi-object filtering algorithms, the quality of the tracking depends heavily on the fidelity of the evolution model describing the objects' dynamics, and this is especially true in the context of SSA where the sensor coverage is poor and opportunities for data corrections are limited. The current evolution model follows a classical design of orbital propagators, in which the perturbation effects that are either omitted or imperfectly modeled are accounted for in an additive, stochastic noise term on the acceleration vector. In this scenario, where the ground truth trajectories are built from real GPS data, the modeling mismatches are significant and must be compensated by a significant level of process noise, leading to a quick degradation of the tracks' state estimates outside of the observation windows. Overall, the orbital evolution model exploited in this paper is unsatisfactory as neither the nature nor the magnitude of the noise term are designed out of physical considerations.

A probabilistic description of the orbital dynamics appears over-descriptive and reflects poorly the limited information we possess on the known perturbation forces, let alone on the *unknown* ones. The alternative representation of uncertain phenomena with *uncertain* variables Houssineau (2018); Houssineau and Bishop (2018), already exploited in this paper for the modeling of a radar with Doppler effect, may reflect more closely the nature of the uncertainty we possess in the orbital propagation. The estimation framework for stochastic populations Houssineau (2015); Houssineau and Clark (2019) is fully compatible with the exploitation of uncertain variables, and the integration of our early works on a single-object filter Delande et al. (2018b) to the filtering architecture presented in this paper is ongoing.

5. Conclusion

This paper presents the HISP filter, a recent multi-object detection/tracking algorithm, in the context of SSA. The HISP filter is a principled Bayesian tracking algorithm whose time- and data-update steps have linear complexity with the number of tracks and the number of collected observations. It was specifically designed for large-scale scenarios with moderately ambiguous track-to-observation associations, motivating our work towards its exploitation to build a catalogue of RSOs. The HISP filter is tested on a scenario involving 115 satellites, whose orbital trajectories are built from real GPS data collected from PlanetLabs' Dove constellation, and two simulated radars with Doppler effect whose generated observations include measurement noise, missed detection, and false positives. A few satellites enter the near-Earth space through scheduled events, but the existence of most of them must be inferred by the HISP filter from the collected observations. Overall, the HISP filter proves reactive in the confirmation of new tracks and the estimation of the size of the constellation, and shows good performance in maintaining track custody. The running time confirms the linear complexity of the time- and data-update steps, and suggests that the HISP filter is a promising candidate for the construction of a large-scale detection/tracking architecture.

References

Bar-Shalom, Y., Li, X., 1995. Multitarget-multisensor Tracking: Principles and Techniques. Bar-Shalom, Y.

Blackman, S. S., Jan. 2004. Multiple Hypothesis Tracking for Multiple Target Tracking. Aerospace and Electronic Systems Magazine, IEEE, 5–18.

Delande, E. D., Frueh, C., Franco, J., Houssineau, J., Clark, D. E., 2018a. Novel Multi-Object Filtering Approach For Space Situational Awareness. Journal of Guidance, Control, and Dynamics 41 (1), 59–73.

Delande, E. D., Houssineau, J., Clark, D. E., 2016. Multi-object filtering with stochastic populations. ArXiv preprint, arXiv:1501.04671v2.

Delande, E. D., Houssineau, J., Franco, J., Frueh, C., Clark, D. E., Feb. 2017. A new multi-target tracking algorithm for a large number of orbiting objects. In: 2017 AAS/AIAA Spaceflight Mechanics Meeting.

Delande, E. D., Houssineau, J., Jah, M. K., Jul. 2018b. A new representation of uncertainty for data fusion in SSA detection and tracking problems. In: Information Fusion, Proceedings of the 21st International Conference on.

Delande, E. D., Houssineau, J., Jah, M. K., 2018c. Physics and human-based information fusion for improved resident space object tracking. Advances in Space Research 62 (7), 1800–1812.

DeMars, K. J., Hussein, I. I., Frueh, C., Jah, M. K., Erwin, R. S., 2015. Multiple-Object Space Surveillance Tracking Using Finite-Set Statistics. Journal of Guidance, Control, and Dynamics 38 (9), 1741–1756.

DeMars, K. J., Jah, M. K., 2013. Probabilistic Initial Orbit Determination Using Gaussian Mixture Models. Journal of Guidance, Control, and Dynamics 36 (5), 1324–1335.

Doucet, A., de Freitas, N., Gordon, N., 2001. Sequential Monte Carlo Methods in Practice. Statistics for Engineering and Information Science. Springer.

Evensen, G., 2004. Sampling strategies and square root analysis schemes for the EnKF. Ocean dynamics 54 (6), 539–560.

Faber, W., Chakravorty, S., Hussein, I. I., Jul. 2016. Multi-object tracking with multiple birth, death, and spawn scenarios using a randomized hypothesis generation technique (RFISST). In: Information Fusion, Proceedings of the 19th International Conference on. pp. 154–161.

Franco, J., Delande, E. D., Frueh, C., Houssineau, J., Clark, D. E., Mar. 2016. A Spherical Co-ordinate Space Parameterisation for Orbit Estimation. In: IEEE 2016 Aerospace Conference. pp. 1–12.

Goodman, I. R., Mahler, R. P. S., Nguyen, H.-T., 1997. Mathematics of Data Fusion. Kluwer Academic Publishers.

Horwood, J. T., Aragon, N. D., Poore, A. B., nov-dec 2011. Gaussian Sum Filters for Space Surveillance: Theory and Simulations. Journal of Guidance, Control, and Dynamics 34 (6), 1839–1851.

Horwood, J. T., Poore, A. B., 2014. Gauss von Mises Distribution for Improved Uncertainty Realism in Space Situational Awareness. SIAM/ASA Journal on Uncertainty Quantification 2, 276–304.

Houssineau, J., 2015. Representation and estimation of stochastic populations. Ph.D. thesis, Heriot Watt University.

Houssineau, J., 2018. Parameter estimation with a class of outer probability measures. arXiv preprint, arXiv:1801.00569.

Houssineau, J., Bishop, A., 2018. Smoothing and filtering with a class of outer measures. SIAM/ASA Journal on Uncertainty Quantification 6 (2), 845–866.

Houssineau, J., Clark, D. E., 2018. Multi-target filtering with linearised complexity. Signal Processing, IEEE Transactions on 66 (18), 4957–4970.

Houssineau, J., Clark, D. E., 2019. On a representation of partially-distinguishable populations. submitted, arXiv:1608.00723v2.

Hussein, I. I., DeMars, K. J., Frueh, C., Erwin, R. S., Jah, M. K., Jul. 2012. An AEGIS-FISST integrated detection and tracking approach to Space Situational Awareness. In: Information Fusion, Proceedings of the 15th International Conference on. pp. 2065–2072.

Jones, B. A., Vo, B.-N., Jan. 2015. A Labelled Multi-Bernoulli Filter for Space Object Tracking. In: 2015 AAS/AIAA Spaceflight Mechanics Meeting. pp. AAS 15–413.

Jones, B. A., Vo, B.-T., Vo, B.-N., Sep. 2016. Generalized Labeled Multi-Bernoulli Space-Object Tracking with Joint Prediction and Update. In: AAS/AIAA Astrodynamics Specialist Conference.

Mahler, R. P. S., 2007. Statistical Multisource-Multitarget Information Fusion. Artech House.

Reid, D., 1979. An Algorithm for Tracking Multiple Targets. Automatic Control, IEEE Transactions on 24 (6), 843–854.

Skolnik, M., 1979. Introduction to Radar Systems, 2nd Edition. McGraw-Hill.

Vo, B.-T., Vo, B.-N., 2013. Labeled Random Finite Sets and Multi-Object Conjuguate Priors. Signal Processing, IEEE Transactions on 61 (13), 3460–3475.

Washburn, R. P., 1987. A Random Point Process Approach to Multiobject Tracking. In: American Control Conference.

Appendix A. Specific operations

Appendix A.1. Merging unidentified objects

Suppose that one wishes to aggregate the information on all the sub-populations of unidentified objects that have entered the scene across the different epochs. At time t, one can merge all these sub-populations in the track $\mathrm{u}_{t|t-1}$ characterized by:

$$\begin{cases} p_{t|t-1}^{\mathrm{u}_{t|t-1}}(x) \propto n_{m_t^{\mathrm{ub}}} q_{m_t^{\mathrm{ub}}}(x) \\ \qquad\qquad + n_{t-1}^{\mathrm{u}_{t-1}} \displaystyle\int \sum_{m \in M_{t-1}^{\mathrm{e}}} q_m(x|x') p_{t-1}^{\mathrm{u}_{t-1}}(x') \mathrm{d}x', \\ w_{t|t-1}^{\mathrm{u}_{t|t-1}} = \dfrac{n_{t-1}^{\mathrm{u}_{t-1}} w_{t-1}^{\mathrm{u}_{t-1}} \displaystyle\int \sum_{m \in M_{t-1}^{\mathrm{e}}} p_m(x) p_{t-1}^{\mathrm{u}_{t-1}}(x) \mathrm{d}x}{n_{t-1}^{\mathrm{u}_{t-1}} + n_{m_t^{\mathrm{ub}}}} \\ \qquad\qquad + \dfrac{n_{m_t^{\mathrm{ub}}} w_{m_t^{\mathrm{ub}}}}{n_{t-1}^{\mathrm{u}_{t-1}} + n_{m_t^{\mathrm{ub}}}}, \\ n_{t|t-1}^{\mathrm{u}_{t|t-1}} = n_{t-1}^{\mathrm{u}_{t-1}} + n_{m_t^{\mathrm{ub}}}. \end{cases} \tag{A.1}$$

In essence, the merged p.d.f. $p_{t|t-1}^{\mathrm{u}_{t|t-1}}$ in (A.1) averages out the evolution models M_{t-1}^{e} in order to predict the evolution of the pre-existing objects, then mix the resulting p.d.f. with the information on the newly-entered objects. Note that the unidentified objects that have entered and left the scene without ever being detected are not represented, since there is little operational gain to maintain information on them. If we omit the information on unidentified objects from past epochs as well,[12] (A.1) yields the approximated form (13).

Appendix A.2. Merging probability distributions

Suppose that, at time $t-1$, the set $\mathbb{K}_{t-1}$ denotes a partition of the track indices $\mathbb{I}_{t-1}$ representing the merging of distributions. That is, a common probability distribution p_{t-1}^{K} represents each track in a subset $K \in \mathbb{K}_{t-1}$. If we denote by $\hat{\mathbb{K}}_t$ the transformation of the partition $\mathbb{K}_{t-1}$ following the time-update and data-update steps, then by construction $\hat{\mathbb{K}}_t$ is a partition of the updated set of tracks $\mathbb{I}_t$. A coarser partition $\mathbb{K}_t \supseteq \hat{\mathbb{K}}_t$, taking advantage of new merging opportunities, can then be formed as follows:

(i) Define $\mathbb{K}_t = \emptyset$ and $L = \emptyset$,

(ii) Find the partition element of highest weight $K^* = \operatorname{argmax}_{K \in \hat{\mathbb{K}}_t \setminus L} \sum_{i \in K} w_t^i$ and define L' as the set containing all the partition elements $K \in \hat{\mathbb{K}}_t \setminus L$ such that the distance $d_{\mathrm{m}}(p_t^K, p_t^{K^*})$, where d_{m} is some appropriate metric, is less than some threshold τ_{m} fixed by the operator. Define the union of track indices $L'' = \{i \in \mathbb{I}_t \text{ s.t. } \exists K \in L', i \in K\}$,

(iii) Merge the probability distributions p_t^K, $K \in L'$, into a common, approximate probability distribution $p_t^{L''}$,

(iv) Redefine L as $L \cup L'$ and $\mathbb{K}_t$ as $\mathbb{K}_t \cup \{L''\}$,

(v) Return to step (ii) until $L = \hat{\mathbb{K}}_t$.

[12] More formally, we make the additional assumption that unidentified births are detected with probability one: since each object is supposed detected upon entering the scene, it is immediately distinguishable and thus the population of indistinguishable objects is empty following each data-update step.

Appendix B. Pseudocode

Algorithm 1 Time-update at time t

1: 1. Initialization: Set $\mathbb{I}_{t|t-1}, \mathbb{I}_t^{\mathrm{d}} \leftarrow \emptyset$
2: 2. Identified objects still in the scene at $t-1$:
3: **for** $(\mathbf{b}_{t-1}, \mathbf{o}_{t-1}) \in \mathbb{I}_{t-1}$ **do**
4: **for** $m \in M_t^{\mathrm{e}}$ **do**
5: Set $\mathbb{I}_{t|t-1} \leftarrow \mathbb{I}_{t|t-1} \cup \{((\mathbf{b}_{t-1}, m), \mathbf{o}_{t-1})\}$
6: Set $p_{t|t-1}^{((\mathbf{b}_{t-1},m),\mathbf{o}_{t-1})}$ with (5)
7: Set $w_{t|t-1}^{((\mathbf{b}_{t-1},m),\mathbf{o}_{t-1})}$ with (10)
8: Set $\mathbb{I}_t^{\mathrm{d}} \leftarrow \mathbb{I}_t^{\mathrm{d}} \cup \{((\mathbf{b}_{t-1}, m_t^{\mathrm{d}}), (\mathbf{o}_{t-1}, \phi)\}$
9: Set $w_{t|t-1}^{((\mathbf{b}_{t-1},m_t^{\mathrm{d}}),\mathbf{o}_{t-1})}$ with (10)
10: 3. Identified births since $t-1$:
11: **for** $m \in M_t^{\mathrm{b}}$ **do**
12: Set $\mathbb{I}_{t|t-1} \leftarrow \mathbb{I}_{t|t-1} \cup \{((\boldsymbol{m}_{t-1}^{\psi}, m), \boldsymbol{\phi}_{t-1})\}$
13: Set $p_{t|t-1}^{((\boldsymbol{m}_{t-1}^{\psi},m),\boldsymbol{\phi}_{t-1})}$ with (11)
14: Set $w_{t|t-1}^{((\boldsymbol{m}_{t-1}^{\psi},m),\boldsymbol{\phi}_{t-1})}$ with (11)
15: 4. Unidentified objects:
16: Set $\mathbb{I}_{t|t-1} \leftarrow \mathbb{I}_{t|t-1} \cup \{\mathrm{u}_{t|t-1}\}$
17: Set $p_{t|t-1}^{\mathrm{u}_{t|t-1}}, n_{t|t-1}^{\mathrm{u}_{t|t-1}}, w_{t|t-1}^{\mathrm{u}_{t|t-1}}$ with (A.1) or (13)
18: 5. Identified objects out of the scene by $t-1$:
19: **for** $(\mathbf{b}_{t-1}, \mathbf{o}_{t-1}) \in \mathbb{I}_{t-1}^{\mathrm{d}}$ **do**
20: Set $\mathbb{I}_t^{\mathrm{d}} \leftarrow \mathbb{I}_t^{\mathrm{d}} \cup \{((\mathbf{b}_{t-1}, m^{\psi}), (\mathbf{o}_{t-1}, \phi))\}$
21: Set $w_t^{((\mathbf{b}_{t-1},m^{\psi}),(\mathbf{o}_{t-1},\phi))} \leftarrow w_{t-1}^{(\mathbf{b}_{t-1},\mathbf{o}_{t-1})}$

Algorithm 2 Data-update at time t

1: 1. Initialization: Set $c_t(\phi), \mathrm{Prod}(c_t), \mathrm{Prod}(\phi) \leftarrow 1$, Set $\mathrm{Norm}(\phi) \leftarrow 0$, Set $\mathbb{I}_t, \mathbb{I}_t^{\mathrm{fp}} \leftarrow \emptyset$
2: 2. Missed detection weights:
3: **for** $i \in \mathbb{I}_{t|t-1} \setminus \mathrm{u}_{t|t-1}$ **do**
4: Set $\breve{w}_t^{i,\phi}, w_t^{i,\phi}$ with (15), Set $\mathrm{Sum}(i) \leftarrow w_t^{i,\phi}$
5: Set $\breve{w}_t^{\mathrm{u}_{t|t-1},\phi}, w_t^{\mathrm{u}_{t|t-1},\phi}$ with (15)
6: Set $\mathrm{Term}(\mathrm{u}_{t|t-1}, \phi) \leftarrow w_t^{\mathrm{u}_{t|t-1},\phi}$
7: 3. Observation terms:
8: **for** $z \in Z_t$ **do**
9: Set $\mathrm{Prod}(z) \leftarrow 1$, Set $\mathrm{Norm}(z) \leftarrow 0$
10: Set $\breve{w}_t^{\mathrm{u}_{t|t-1},z}, w_t^{\mathrm{u}_{t|t-1},z}$ with (15)
11: Set $c_t(z)$ with (19)
12: Set $\mathrm{Prod}(c_t) \leftarrow \mathrm{Prod}(c_t)c_t(z)$
13: **for** $i \in \mathbb{I}_{t|t-1} \setminus \mathrm{u}_{t|t-1}$ **do**
14: Set $\breve{w}_t^{i,z}, w_t^{i,z}$ with (15)
15: Set $\mathrm{Sum}(i) \leftarrow \mathrm{Sum}(i) + w_t^{i,z}/c_t(z)$

Algorithm 2 Data-update at time t (cont.)

16: 4. Track terms:
17: **for** $i \in \mathbb{I}_{t|t-1} \setminus \mathrm{u}_{t|t-1}$ **do**
18: Set $\mathrm{Term}(i, \phi) \leftarrow \mathrm{Sum}(i)$
19: Set $\mathrm{Prod}(\phi) \leftarrow \mathrm{Prod}(\phi)\mathrm{Sum}(i)$
20: **for** $z \in Z_t$ **do**
21: Set $\mathrm{Term}(i, z) \leftarrow \mathrm{Sum}(i) - w_t^{i,z}/c_t(z)$
22: Set $\mathrm{Prod}(z) \leftarrow \mathrm{Prod}(z)\mathrm{Term}(i, z)$
23: 5. External weights:
24: **for** $i \in \mathbb{I}_{t|t-1}$ **do**
25: **for** $z \in \bar{Z}_t$ **do**
26: Set $w_{\mathrm{ex}}^{i,z} \leftarrow \frac{\mathrm{Prod}(c_t)\mathrm{Prod}(z)}{c_t(z)\mathrm{Term}(i,z)}$
27: Set $\mathrm{Norm}(z) \leftarrow \mathrm{Norm}(z) + w_{\mathrm{ex}}^{i,z} w_t^{i,z}$
28: **for** $z \in Z_t$ **do**
29: Set $w_{\mathrm{ex}}^{\mathrm{fp},z} \leftarrow \mathrm{Prod}(c_t)\mathrm{Prod}(z)/(1 - p_{t|t-1}^{\mathrm{fp}}(z))$
30: Set $\mathrm{Norm}(\mathrm{fp}, z) \leftarrow \mathrm{Norm}(z) + w_{\mathrm{ex}}^{\mathrm{fp},z} p_{t|t-1}^{\mathrm{fp}}(z)$
31: 6. Objects identified by $t-1$:
32: **for** $(\mathbf{b}_t, \mathbf{o}_{t-1}) \in \mathbb{I}_{t|t-1} \setminus \mathrm{u}_{t|t-1}$ **do**
33: **for** $z \in \bar{Z}_t$ **do**
34: Set $\mathbb{I}_t \leftarrow \mathbb{I}_t \cup \{(\mathbf{b}_t, (\mathbf{o}_{t-1}, z))\}$
35: Set $p_t^{(\mathbf{b}_t,(\mathbf{o}_{t-1},z))}$ with (6)
36: Set $w_t^{(\mathbf{b}_t,(\mathbf{o}_{t-1},z))} \leftarrow \frac{w_{\mathrm{ex}}^{(\mathbf{b}_t,\mathbf{o}_{t-1}),z} \breve{w}_t^{(\mathbf{b}_t,\mathbf{o}_{t-1}),z}}{\mathrm{Norm}(z)}$
37: 7. Objects identified since $t-1$:
38: **for** $z \in Z_t$ **do**
39: Set $\mathbb{I}_t \leftarrow \mathbb{I}_t \cup \{(m_{0:t}^{\mathrm{ub}}, (\boldsymbol{\phi}_{t-1}, z))\}$
40: Set $p_t^{(m_{0:t}^{\mathrm{ub}},(\boldsymbol{\phi}_{t-1},z))}$ with (6)
41: Set $w_t^{(m_{0:t}^{\mathrm{ub}},(\boldsymbol{\phi}_{t-1},z))} \leftarrow \frac{w_{\mathrm{ex}}^{\mathrm{u}_{t|t-1},z} \breve{w}_t^{\mathrm{u}_{t|t-1},z}}{\mathrm{Norm}(z)}$
42: 8. False positives up to $t-1$:
43: **for** $(\mathbf{b}_{t-1}, \mathbf{o}_{t-1}) \in \mathbb{I}_{t-1}^{\mathrm{fp}}$ **do**
44: Set $\mathbb{I}_t^{\mathrm{fp}} \leftarrow \mathbb{I}_t^{\mathrm{fp}} \cup \{((\mathbf{b}_{t-1}, m^{\psi}), (\mathbf{o}_{t-1}, \phi))\}$
45: Set $w_t^{((\mathbf{b}_{t-1},m^{\psi}),(\mathbf{o}_{t-1},\phi))} \leftarrow w_{t-1}^{(\mathbf{b}_{t-1},\mathbf{o}_{t-1})}$
46: 9. False positives since $t-1$:
47: **for** $z \in Z_t$ **do**
48: Set $\mathbb{I}_t^{\mathrm{fp}} \leftarrow \mathbb{I}_t^{\mathrm{fp}} \cup \{(\boldsymbol{m}_t^{\psi}, (\boldsymbol{\phi}_{t-1}, z))\}$
49: Set $w_t^{(\boldsymbol{m}_t^{\psi},(\boldsymbol{\phi}_{t-1},z))} \leftarrow \frac{w_{\mathrm{ex}}^{\mathrm{fp},z} p_{t|t-1}^{\mathrm{fp}}(z)}{\mathrm{Norm}(\mathrm{fp},z)}$

Appendix C. SMC implementation

Appendix C.1. Probability distributions for orbiting objects

Representing the uncertainty on the kinematic state of a RSO with a probability distribution is not straightforward. The peculiar shape of uncertainty regions on orbiting objects is ill-approximated with simple parameterized functions such a single Gaussian distribution. Parameterized distributions present additional difficulties for the time-update step; indeed, the orbital propagation of a kinematic state is relatively easy to implement through well-established, empirical methods, but the propagation of parameters of a different nature – such as the statistical moments of a probability distribution – remains challenging when complex perturbations effects are taken into account. Several approaches have been proposed in the context of SSA, such as Gaussian sum filters Horwood et al. (2011) or Gauss von Mises distributions Horwood and Poore (2014); other solutions, such as the ensemble Kalman filter Evensen (2004), appear promising as well.

Following our previous works on SSA applications Delande et al. (2018a, 2017, 2018c), we represent instead probability distributions with sets of weighted particles Doucet et al. (2001). By construction, a track $i \in \mathbb{I}_t$ represents an object that is still in the scene, i.e., their probability distribution p_t^i on the extended object state space $\bar{\mathbf{X}}$ has no mass on the "away" state ψ. Thus, p_t^i can be approximated by the set of weighted particles $\{\gamma_t^{i,(j)}, x_t^{i,(j)}\}_{j=1}^J$, such that

$$p_t^i(x) \simeq \sum_{j=1}^{J} \gamma_t^{i,(j)} \delta_{x_t^{i,(j)}}(x), \tag{C.1}$$

for any $x \in \mathbf{X}$, where $\delta_{x_t^{i,(j)}}$ is the Dirac delta function at $x_t^{i,(j)} \in \mathbf{X}$, and with $\sum_{j=1}^J \gamma_t^{i,(j)} = 1$.

Appendix C.2. Time-update step

We describe here the evolution model m_t^{e} corresponding to a stable, LEO trajectory. We denote by T_t the epoch, measured in seconds since the J2000 reference, at time step $t \in \mathbb{N}$. Given a RSO evolving on a closed orbit, with kinematic state $x = (\mathbf{p}(T), \mathbf{v}(T))$ at some epoch T, the component of its acceleration vector $\dot{\mathbf{v}}(T)$ due to the modeled perturbations is denoted by the mapping

$$\mathbf{a}_{\mathrm{mod.}}(\mathbf{p}(T), \mathbf{v}(T), T), \tag{C.2}$$

which includes the central term of Earth's gravitational pull, the zonal/tesseral effects up to order and degree 20, the gravitational pull of the Sun and the Moon, the solar radiation pressure (for an AMR of $0.0015\,\mathrm{m^2\,kg^{-1}}$, and a spherical shape with a radiation pressure coefficient of 0.3), and a drag term based on the MSIS86 atmospheric model (for a ballistic coefficient of $25\,\mathrm{kg\,m^{-2}}$). Non-modeled perturbations are accounted for in an additional term

$$\begin{aligned}&\mathbf{a}_\epsilon(\mathbf{p}(T), \mathbf{v}(T), T, \boldsymbol{\omega}(T_{t-1})) \\ &\qquad = f^{\mathrm{eci}}_{\mathrm{ric}(\mathbf{p},\mathbf{v})}\left((T - T_{t-1})\boldsymbol{\omega}(T_{t-1})\right),\end{aligned} \tag{C.3}$$

where $\boldsymbol{\omega}$ is a zero-mean Gaussian noise with standard deviation $10^{-6}\,\mathrm{m\,s^{-3}}$ on each component in the object's RIC frame, and $f^{\mathrm{eci}}_{\mathrm{ric}(\mathbf{p},\mathbf{v})}$ is the mapping that transforms a vector in the object's RIC frame to the reference ECI frame. The total acceleration term describing the orbital dynamics is then given by the sum

$$\begin{aligned}&\mathbf{a}_{\mathrm{orb.}}\left(\mathbf{p}(T), \mathbf{v}(T), T, \boldsymbol{\omega}(T_{t-1})\right) = \\ &\mathbf{a}_{\mathrm{mod.}}\left(\mathbf{p}(T), \mathbf{v}(T), T\right) + \mathbf{a}_\epsilon\left(\mathbf{p}(T), \mathbf{v}(T), T, \boldsymbol{\omega}(T_{t-1})\right),\end{aligned} \tag{C.4}$$

so that the time-derivative $\dot{x}$ of the RSO's state is given by

$$(\dot{\mathbf{p}}(T), \dot{\mathbf{v}}(T)) = \left(\mathbf{v}(T), \mathbf{a}_{\mathrm{orb.}}\left(\mathbf{p}(T), \mathbf{v}(T), T, \boldsymbol{\omega}(T_{t-1})\right)\right). \tag{C.5}$$

Let $i = (\mathbf{b}_{t-1}, \mathbf{o}_{t-1}) \in \mathbb{I}_{t-1} \setminus \{\mathrm{u}_{t-1}\}$ be a distinguishable track, with probability distribution approximated by the weighted particle set $\left\{\gamma_{t-1}^{i,(j)}, x_{t-1}^{i,(j)}\right\}_{j=1}^J$. Following the time-update formula (5), the probability distribution of the predicted track $i' = ((\mathbf{b}_{t-1}, m_t^{\mathrm{e}}), \mathbf{o}_{t-1})$ is then approximated by the particle set $\left\{\gamma_{t|t-1}^{i',(j)}, x_{t|t-1}^{i',(j)}\right\}_{j=1}^J$ with

$$\begin{cases} \gamma_{t|t-1}^{i',(j)} &= \gamma_{t-1}^{i,(j)}, \\ x_{t|t-1}^{i',(j)} &= x_{t-1}^{i,(j)} + \displaystyle\int_{T_{t-1}}^{T_t} \left(\mathbf{v}^{i,(j)}(T), \mathbf{a}_{\mathrm{orb.}}^{i,(j)}(T)\right) \mathrm{d}T, \end{cases} \tag{C.6}$$

where

$$\mathbf{a}_{\mathrm{orb.}}^{i,(j)}(T) = \mathbf{a}_{\mathrm{orb.}}\left(\mathbf{p}^{i,(j)}(T), \mathbf{v}^{i,(j)}(T), T, \boldsymbol{\omega}^{i,(j)}(T_{t-1})\right), \tag{C.7}$$

with $x_{t-1}^{i,(j)} = \left(\mathbf{p}^{i,(j)}(T_{t-1}), \mathbf{v}^{i,(j)}(T_{t-1})\right)$, $1 \le j \le J$. Since the stochastic component $\boldsymbol{\omega}^{i,(j)}(T_{t-1})$ is constant throughout the time interval $[T_{t-1}, T_t]$, the integral in (C.6) can be solved with a usual numerical integrator.

Appendix C.3. Data-update step

The radar is modeled with a potential g_t, describing the precision/accuracy of its observation process (7). It is then customary to build the potential $g_t(\cdot|x)$ as a p.d.f. on $\mathbf{Z}_t$, *characterizing* the noise distribution of the sensor. However, the uncertainty in a sensor's observation process originates from limited knowledge in the physical phenomena producing the observation (the imperfections in the radar antenna, the middle between the radar antenna and the object, the reflectivity and orientation of the object, etc.) rather than in a well-studied *random* effect generating the observation. We exploit here a more generalized representation of an uncertain phenomenon based on *uncertain* variables, distinguishing the *epistemic* part reflecting the limited knowledge possessed by an observer of the phenomena, from the *aleatory* part characterizing the phenomenon's inherent randomness, if any Houssineau (2018); Houssineau and Bishop (2018). The potential g_t is built as a dimensionless, non-negative function on $\mathbf{Z}_t$ with supremum one, called a *possibility function* (on $\mathbf{Z}_t$). In particular, the radar is modeled with the *Gaussian possibility function* Houssineau (2018)

$$g_t(z|x) = \exp\left(-\frac{1}{2}(z - H_t f_{\text{eci}}^{\text{top.}}(x))^{\mathrm{T}} R_t^{-1}(z - H_t f_{\text{eci}}^{\text{top.}}(x))\right), \tag{C.8}$$

where $f_{\text{eci}}^{\text{top.}}$ is the mapping from the object state space $\mathbf{X}$ to the sensor's local spherical frame, $H_t = [\boldsymbol{I}_4\ \mathbf{0}_{4,2}]$ is the observation matrix of the sensor, and R_t is the diagonal, noise covariance matrix formed with the standard deviations given in Table 1. The potential $g_t(z|x)$ captures the limited information we possess on the radar, but does not characterize its observation process. If we denote by $\Pr\{z \in Z|x\}$ the probability that the generated observation falls within some subset of sensor cells $Z \subseteq Z_t'$, according to the unknown observation process of the radar and given that the observed object has state $x \in \mathbf{X}$, the possibility (C.8) provides us with the upper bound

$$0 \leq \Pr\{z \in Z|x\} \leq \max_{z \in Z} g_t(z|x), \tag{C.9}$$

but the probability of the event itself remains unknown, in the general case. This alternative representation is particularly convenient to model uncertain components on which information is scarce Delande et al. (2018c,b).

Let $i = (\mathbf{b}_t, \mathbf{o}_{t-1}) \in \mathbb{I}_{t-1} \setminus \{\mathrm{u}_{t-1}\}$ be a distinguishable track, with probability distribution approximated by the weighted particle set $\left\{\gamma_{t|t-1}^{i,(j)}, x_{t|t-1}^{i,(j)}\right\}_{j=1}^{J}$, and let $z \in Z_t$ be a collected observation at time t. Following the data-update formula (6), the p.d.f. of the posterior track $i' = (\mathbf{b}_t, (\mathbf{o}_{t-1}, z))$, corresponding to a detection, can be approximated by the particle set $\left\{\gamma_t^{i',(j)}, x_t^{i',(j)}\right\}_{j=1}^{J}$ with

$$\begin{cases} \tilde{x}_t^{i',(j)} & = x_{t|t-1}^{i,(j)} \\ \tilde{\gamma}_t^{i',(j)} & = \dfrac{p_{\mathrm{d},t}(x_{t|t-1}^{i,(j)}) g_t(z|x_{t|t-1}^{i,(j)}) \gamma_{t|t-1}^{i,(j)}}{\sum_{j'=1}^{J} p_{\mathrm{d},t}(x_{t|t-1}^{i,(j')}) g_t(z|x_{t|t-1}^{i,(j')}) \gamma_{t|t-1}^{i,(j')}}, \end{cases} \tag{C.10}$$

for $1 \leq j \leq J$. While the implementation of the update procedure (C.10) is straightforward, it leads to quick degeneracy among the particles because of the high accuracy of the radar observation and the peakiness of the potential (C.8) Delande et al. (2017, 2018c). In this paper, we exploit instead a parametrization of the predicted p.d.f. $p_{t|t-1}^{i}$ allowing for a more robust data-update mechanism Franco et al. (2016); Delande et al. (2017). Even though the predicted set of weighted particles $\left\{\gamma_{t|t-1}^{i,(j)}, x_{t|t-1}^{i,(j)}\right\}_{j=1}^{J}$ can hardly be approximated as a Gaussian distribution in the object state space $\mathbf{X}$, the Gaussian approximation holds more easily in the sensor's local topocentric frame equipped with spherical coordinates. The data-update procedure can be summarized as follows:

1. Transform $\left\{\gamma_{t|t-1}^{i,(j)}, x_{t|t-1}^{i,(j)}\right\}_{j=1}^{J}$ to sensor's local frame:$\rightarrow \left\{p_{\mathrm{d},t}(x_{t|t-1}^{i,(j)})\gamma_{t|t-1}^{i,(j)}, f_{\text{eci}}^{\text{top.}}(x_{t|t-1}^{i,(j)})\right\}_{j=1}^{J}$,
2. Approximate as a Gaussian distribution: $\rightarrow (\mu_{t|t-1}^{i}, P_{t|t-1}^{i})$,
3. Update Gaussian distribution with potential $g_t(z|\cdot)$: $\rightarrow (\mu_t^{i'}, P_t^{i'})$,
4. Sample resulting distribution: $\rightarrow \left\{J^{-1}, s_t^{i',(j)}\right\}_{j=1}^{J}$,
5. Transform distribution back to the object space $\mathbf{X}$: $\rightarrow \left\{J^{-1}, (f_{\text{eci}}^{\text{top.}})^{-1}(s_t^{i',(j)})\right\}_{j=1}^{J}$.

The p.d.f. $p_t^{i'}$ is then approximated by $\left\{\gamma_t^{i',(j)}, x_t^{i',(j)}\right\}_{j=1}^{J} = \left\{J^{-1}, (f_{\text{eci}}^{\text{top.}})^{-1}(s_t^{i',(j)})\right\}_{j=1}^{J}$. Note that the data-update step in the sensor's

local topocentric frame is a simple linear Kalman update, since the potential $g_t(z|x)$ is modeled with a Gaussian possibility (C.8). This procedure, while robust, incurs a loss of information in the Gaussian approximation step and would require further improvements; it is, however, beyond the scope of this paper. The association weight (15) is then given by

$$w_t^{i,z} = w_{t|t-1}^i \left[\sum_{j=1}^{J} p_{\mathrm{d},t}(x_{t|t-1}^{i,(j)}) \gamma_{t|t-1}^{i,(j)} \right] \times \sqrt{\frac{|R_t|}{|S_{t|t-1}^i|}} \exp\left(-\frac{1}{2} \hat{z}^T (S_{t|t-1}^i)^{-1} \hat{z} \right), \quad \text{(C.11)}$$

where $\hat{z} = H_t \mu_{t|t-1}^i - z$, $|\cdot|$ is the determinant, and $S_{t|t-1}^i = H_t P_{t|t-1}^i H_t^T + R_t$ is the innovation covariance. Following the data-update formula (6), the p.d.f. of the posterior track $i'' = (\mathbf{b}_t, (\mathbf{o}_{t-1}, \phi))$, corresponding to a missed detection, can be approximated by the set of weighted particle $\left\{ \gamma_t^{i'',(j)}, x_t^{i'',(j)} \right\}_{j=1}^{J}$ with

$$\begin{cases} x_t^{i'',(j)} &= x_{t|t-1}^{i,(j)} \\ \gamma_t^{i'',(j)} &= \dfrac{\left[1 - p_{\mathrm{d},t}(x_{t|t-1}^{i,(j)})\right] \gamma_{t|t-1}^{i,(j)}}{\sum_{j'=1}^{J} \left[1 - p_{\mathrm{d},t}(x_{t|t-1}^{i,(j')})\right] \gamma_{t|t-1}^{i,(j')}}, \end{cases} \quad \text{(C.12)}$$

for $1 \leq j \leq J$, and the corresponding association weight (15) is given by

$$w_t^{i,\phi} = w_{t|t-1}^i \left[\sum_{j=1}^{J} \left[1 - p_{\mathrm{d},t}(x_{t|t-1}^{i,(j)})\right] \gamma_{t|t-1}^{i,(j)} \right]. \quad \text{(C.13)}$$

Note that the association weight (C.11) is dimensionless and invariant with arbitrary changes of units on the observation space $\mathbf{Z}_t$, which allows for a straightforward comparison with the missed detection weight (C.13) above. The representation of the potential g_t with a dimensionless Gaussian potential (C.8), rather than a unit-dependent Gaussian p.d.f. on $\mathbf{Z}_t$, thus alleviates potential issues raising from the comparison between unit-dependent detection weights $w_t^{i,z}$ and unit-independent missed detection weights $w_t^{i,\phi}$.

The new track $i''' = \left(m_{0:t}^{\mathrm{ub}}, (\boldsymbol{\phi}_{t-1}, z)\right) \in \mathbb{I}_t$ corresponds to an unidentified object detected for the first time through the collected observation z. Since no prior information is assumed on the spatial distribution of unidentified objects, the p.d.f. $p_t^{i'''}$ is initialized through the admissible region approach developed in DeMars and Jah (2013). We implemented this approach as in our previous works Delande et al. (2017), summarized as follows. An initial set of weighted particles $\left\{ J^{-1}, s_t^{i''',(j)} \right\}_{j=1}^{J}$ is produced in the sensor's local topocentric frame; the observed components $\rho, \theta, \varphi, \dot{\rho}$ are sampled from the collected observation and the sensor's noise covariance matrix R_t, and the unobserved angular rates $\dot{\theta}, \dot{\varphi}$ are sampled uniformly from the admissible region determined in DeMars and Jah (2013). The initial p.d.f. $p_t^{i'''}$ is then approximated with the distribution transported in the object state space $\mathbf{X}$, i.e., with the set of weighted particles $\left\{ \gamma_t^{i''',(j)}, x_t^{i''',(j)} \right\}_{j=1}^{J} = \left\{ J^{-1}, (f_{\mathrm{eci}}^{\mathrm{top.}})^{-1}(s_t^{i''',(j)}) \right\}_{j=1}^{J}$. The association weight (15) is approximated by $w_t^{\mathrm{ub},z} = w_{t|t-1}^{\mathrm{ub}}$ Houssineau and Clark (2018).

Appendix C.4. Assessing the "closeness" of orbital trajectories

In order to assess the "closeness" of probability distributions in the object state space $\mathbf{X}$, describing orbital trajectories, we proceed as follows Delande et al. (2017). Suppose that two p.d.f.s p_t^i, $p_t^{i'}$ are represented by the set of weighted particles $\left\{ \gamma_t^{i,(j)}, x_t^{i,(j)} \right\}_{j=1}^{J}$ and $\left\{ \gamma_t^{i',(j)}, x_t^{i',(j)} \right\}_{j=1}^{J}$, respectively, and we wish to determine if they are close enough for merging purposes. We define the metric between these two distributions as follows:

1. Transform $\left\{ \gamma_t^{i,(j)}, x_t^{i,(j)} \right\}_{j=1}^{J}$ to spherical coordinates: $\rightarrow \left\{ \gamma_t^{i,(j)}, f_{\mathrm{cart.}}^{\mathrm{sph}}(x_t^{i,(j)}) \right\}_{j=1}^{J}$,
2. Transform $\left\{ \gamma_t^{i',(j)}, x_t^{i',(j)} \right\}_{j=1}^{J}$ to spherical coordinates: $\rightarrow \left\{ \gamma_t^{i',(j)}, f_{\mathrm{cart.}}^{\mathrm{sph}}(x_t^{i',(j)}) \right\}_{j=1}^{J}$,
3. Approximate as Gaussian distributions: $\rightarrow (\mu_t^i, P_t^i)$ and $(\mu_t^{i'}, P_t^{i'})$,
4. Compute metric $d_{\mathrm{m}}(p_t^i, p_t^{i'}) = (\mu_t^i - \mu_t^{i'})(P_t^i + P_t^{i'})^{-1}(\mu_t^i - \mu_t^{i'})^T$,

where $f_{\mathrm{cart.}}^{\mathrm{sph}}$ is the mapping from Cartesian to spherical coordinates.

-New multi-target tracking algorithm for orbiting objects
-Filtering has linear complexity with number of tracks and observations
-Track identification process through behavior patterns and/or sensor observations
-Pseudocode is given to guide practical implementation
-Test scenario has 115 satellites based on real data, and two sensors with noise